Combining observed linear basin amplification factors with 1D nonlinear site-response analyses to predict site response for strong ground motions: Application to Wellington, New Zealand

Christopher A de la Torre, M.EERI[1] [iD],
Brendon A Bradley, M.EERI[1] [iD], Felipe Kuncar,
M.EERI[1] [iD], Robin L Lee, M.EERI[1] [iD], Liam M
Wotherspoon, M.EERI[2] [iD], and Anna E Kaiser[3]

Abstract

This study develops a method for estimating site amplification that combines instrumentally observed site-specific amplification factors with adjustment factors from nonlinear site-response analyses. This approach provides estimates of site response for large-strain motions based on observations and sophisticated nonlinear modeling. A database of weak-to-moderate intensity ground motions recorded in three basins of Wellington, New Zealand is used to study the observed site amplification. A subset of nine strong-motion stations was selected to perform nonlinear site-response analyses with scaled strong ground motions to assess the influence of nonlinearity on site amplification factors and demonstrate the approach. Different shear-wave velocity (V_S) profiles, constitutive models, and modeling approaches (e.g. one-dimensional (1D) site-response analyses vs empirical V_{S30}-based approaches) are used to quantify the sensitivity and modeling uncertainty in the nonlinear site-response analyses. It was found that for soft sites subjected to strong ground motions, there may be a decrease in spectral acceleration amplification factors for periods up to approximately 2 s, relative to the expected linear site response. For longer periods, there is little to no amplification from the effects of soil nonlinearity. However, at stiffer sites,

[1]Civil and Natural Resources Engineering, University of Canterbury, Christchurch, New Zealand
[2]Civil and Environmental Engineering, University of Auckland, Auckland, New Zealand
[3]GNS Science, Lower Hutt, New Zealand

Corresponding author:
Christopher A de la Torre, Civil and Natural Resources Engineering, University of Canterbury, Private Bag 4800, Christchurch 8140, New Zealand.
Email: christopher.delatorre@canterbury.ac.nz

which generally experience less basin amplification in observations, there may be moderate amplification at longer periods when nonlinearity is considered due to softening of the soil profile. Empirical ground-motion models were found to under-represent the observed amplification between basin sites and the nearby reference site, especially at intermediate to long periods, corresponding to resonant frequencies of these basin sites. In addition, the empirical nonlinear site amplification models (V_{S30}-based) were found to deviate from nonlinear analyses at large strains, where such models are poorly constrained due to such a limited number of observations.

Introduction

Observations from past earthquakes have shown that sedimentary basins and soft surficial soils can cause large amplification of seismic waves (e.g. Bradley et al., 2018; Frankel et al., 2002), producing strong shaking at the ground surface. With increasing density of seismic instrumentation, it is becoming possible to use region- or site-specific estimates of site response based on observations to develop, or critique, ground-motion and site-response modeling procedures (e.g. de la Torre et al., 2020; Lee et al., 2020; Nweke et al., 2022a; Parker and Baltay, 2022; Zhu et al., 2020). Some of these modeling techniques, such as empirically derived ground-motion models (GMMs), three-dimensional (3D) ground-motion simulations, and corrected horizontal-to-vertical spectral ratio (HVSR) techniques have been found to predict site and basin response with reasonable accuracy (e.g. Bradley et al., 2017; Day et al., 2019; Graves and Pitarka, 2015; Nweke et al., 2022b; Zhu et al., 2022). One of the challenges of these procedures is the handling of soil nonlinearity and its influence on site amplification. This is due to the lack of instrumental observations of strong nonlinearity in site response, and the inability for some of these methods to model complex site-specific nonlinear site response.

The Wellington region in New Zealand is a high seismicity zone that is strongly influenced by the site response in sedimentary basins. The Wellington Central Business District (CBD) and the nearby city of Lower Hutt are underlain by fault-bounded sedimentary basins (Kaiser et al., 2020) that have been shown to appreciably amplify ground motions in the period range of $T = 0.5 - 3s$ (Adams et al., 2012; Bradley et al., 2018; Kaiser et al., 2020). Modeling and analysis of observations have further demonstrated that softer, deeper soil sites around the port and waterfront produce additional site amplification compared with nearby stiffer or shallower soil sites (Cubrinovski et al., 2018; Kaiser et al., 2012). This amplification played a key role in the damage pattern observed after the 2016 Kaikōura earthquake, where several mid- to high-rise buildings were severely affected (Bradley et al., 2018; Cubrinovski et al., 2018). Given that the majority of recorded events in the Wellington region are weak ground motions, a question that arises is whether the amplification factors computed from these observations are suitable for use with stronger, design-level, earthquake scenarios. One of the challenges faced globally for ground-motion prediction of strong ground-motions, which are of engineering interest, is the lack of observations of strong motions from a wide distribution of site, basin, path, and earthquake characteristics; this results in generally poorly constrained models in the range of

ground motions that is of highest interest to engineers, policymakers, emergency managers, and others.

To overcome challenges arising from limited observations of strong ground motions, approaches coupling observations with simulations, or different simulation methods have been proposed. For example, Bazzurro and Cornell (2004) developed a framework to use site-specific one-dimensional (1D) nonlinear site-response analyses to adjust hazard curves from empirical models, while de la Torre et al. (2020) and Pilz et al. (2021) used 1D site-response analyses to modify ground motions from regional-scale 3D ground-motion simulations which are currently incapable of capturing smaller-scale site-specific features and soil nonlinearity. Stewart et al. (2017) proposed using observations of linear site response in combination with 1D nonlinear site-response analyses to estimate the influence of site effects on ground motions for larger ground-motion amplitudes than what has been instrumentally observed at the site. In a similar manner, this study proposes combining site-specific site response from weak ground motion observations with 1D total stress nonlinear site-response analyses to estimate how these amplification factors vary with increasing ground-motion intensity. A database of weak-to-moderate intensity ground motions recorded in three basins of Wellington, New Zealand is used to study the observed site amplification. A subset of nine strong-motion stations was selected to perform nonlinear site-response analyses with strong ground motions to assess the influence of nonlinearity on site amplification factors and demonstrate the approach.

Methodology

Sites considered and basins in the Wellington region

Site-response observations are estimated from ground motion recordings at 43 strong-motion stations (SMS) throughout three main sedimentary basins of Wellington, New Zealand. The Te Aro and Thorndon basins are located in the Central Business District of Wellington and a third deeper basin exists under the cities of Lower Hutt and Petone. The map of the greater Wellington region in Figure 1 plots the estimated elevation (relative to mean sea level) of bedrock in the Wellington region (Hill et al., 2022) and identifies these basins of interest. A subset of nine stations, with good geotechnical and geophysical site characterization data (generally seismic cone penetration testing (sCPT), and active and passive surface wave methods), were selected for nonlinear site-response analyses with strong ground motions to assess the influence of nonlinearity on site/basin amplification factors and demonstrate the approach.

Figure 2 shows the location of all SMS in the two regions (Wellington and Lower Hutt), as well as the surface traces of the Wellington and Aotea faults. The SMS symbols are color-coded by site period, showing values as long as 2 s in the deepest portions of the Lower Hutt basin. Table 1 includes additional metadata for all sites such as the time-averaged shear-wave velocity in the upper 30 m (V_{S30}), the "site period," which represents the fundamental period of the soil profile above rock or the resonant period from strong topographic amplification effects at rock sites, based on the peak of microtremor horizontal-to-vertical spectral ratio measurements (T_{site}; for more details see Wotherspoon et al., 2022), and the depth to $V_S = 1000$m/s ($Z_{1.0}$). Current basin models for the Wellington and Hutt regions estimate the maximum depth to bedrock as approximately 150, 350, and 350 m for Te Aro, Thorndon, and Lower Hutt basins, respectively (Kaiser et al., 2019). The site period estimates shown in Figure 2 reflect this trend with increasing depth (i.e. increasing site period with increasing basin depth).
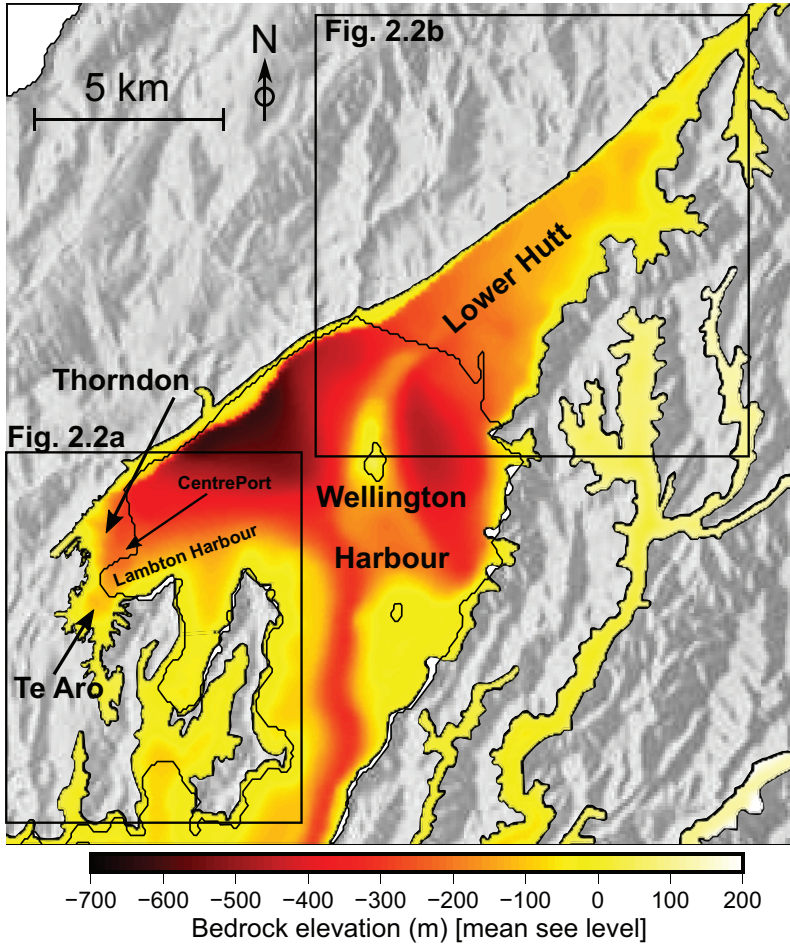
Figure 1. Estimates of bedrock elevation (relative to mean sea level) from the Hill et al. (2022) 3D Wellington Basin model. The main sub-basins of interest in this study are identified (Thorndon, Te Aro, and Lower Hutt).

Shear wave velocity (V_S) profiles for the nine stations at which nonlinear site-response analyses were performed are plotted in Figure 3. The profiles are based on surface wave testing by Vantassel et al. (2018) (PIPS, CPLB, WEMS, TEPS, VUWS, FKPS), and unpublished sCPT and surface wave testing by the authors (WNAS, MISS, CPLB, PIPS, WNKS). From top-left to bottom-right, the sites are ordered by T_{site}, which generally illustrates an increase in profile depth to reach 500 m/s and/or a decrease in V_S in the near surface. The profiles range from 18 to 120 m deep, and some sites have soft silt/clay layers with V_S as low as $100 - 120$ m/s. Vantassel et al. (2018) provided profiles using different layering ratio assumptions (layering ratio is inversely proportional to number of layers). Given these different layering ratio assumptions and high-quality sCPT estimates at some sites, there are two or more V_S profiles for most sites.

Ground-motion database

A subset of ground motions from the 2021 New Zealand Ground Motion Database (Hutchinson et al., 2021) was used for this study. All events recorded at any of the 42
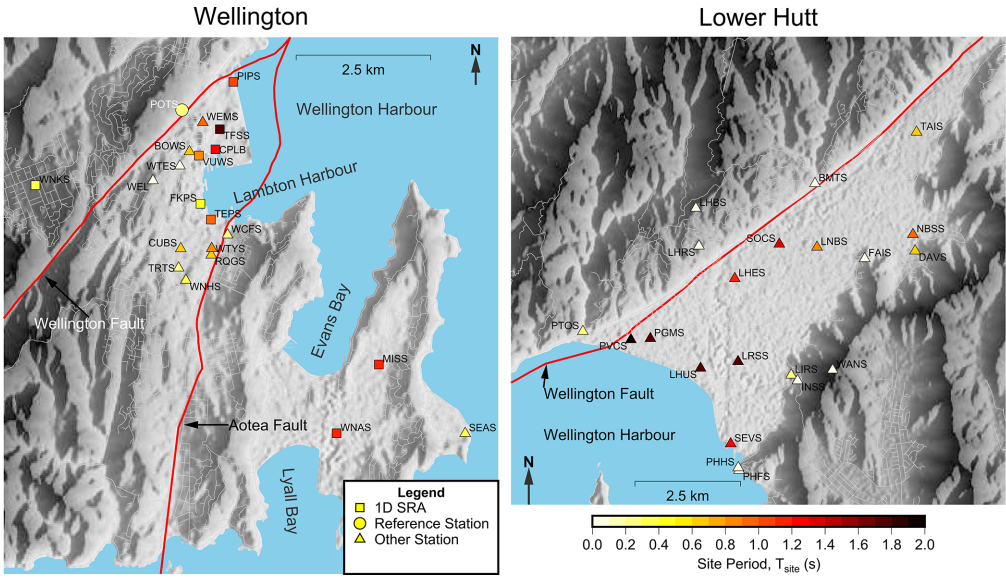
Figure 2. Topographic maps showing the location of strong motion stations used for this study in Wellington (left) and Lower Hutt (right). Station markers are color-coded by site period based on Wotherspoon et al. (2022). Stations in Wellington at which nonlinear site-response analyses (SRA) were performed are plotted with square symbols, and the reference station (POTS) is plotted with a circle and white font.

stations and the reference station (POTS) simultaneously were included in this study. The ground-motion preprocessing is documented in Hutchinson et al. (2021), however, additional rejection criteria on the database were enforced. These criteria help ensure that only the highest quality records within the selected moment magnitude (M_w) and source-to-site distance (R_{rup}) ranges are used. The aim was to achieve a reasonable tradeoff between data quantity and alignment with applicable ranges of empirical GMMs used. Only the ground motions meeting the following criteria were accepted into the dataset used for this study:

- Crustal events with $R_{rup} \leqslant 300.0$ km and $M_w \geqslant 3.5$;
- Interface subduction events with $R_{rup} \leqslant 500.0$ km and $M_w \geqslant 4.5$;
- Slab subduction events with $R_{rup} \leqslant 500.0$ km and $M_w \geqslant 4.5$;
- Accelerometer channels only (i.e. "HN" and "BN" channels).

Following the additional rejection criteria, a total of 74 events, with weak-to-moderate shaking intensities, were available at POTS, making that the maximum possible number of events considered for any site. The total number of event and site pairs in the database used for this study was 1528. The number of events considered for each site (N_E) is listed in Table 1. Figure 4 shows the distribution of M_w for the events recorded at POTS. The map in Figure 5 plots the location of all stations and events (epicenters) considered and shows that many of these events are located in the Cook Strait and the northeast (NE) corner of the South Island.

Table 1. Metadata for Wellington region SMS including maximum and geometric mean observed horizontal PGA (geometric mean of two orthogonal components and all events recorded at the site)

SMS ID	Lat.	Lon.	$Z_{1.0}$(m)	T_{site} (s)	V_{S30}(m/s)	Max. PGA (g)	Mean PGA (g)	N_E
BMTS	−41.19137	174.92603	15	0.05	1000	0.084	0.002	54
BOWS	−41.27919	174.77632	65	0.62	267	0.162	0.008	36
CPLB	−41.27881	174.78209	247	1.21	244	0.267	0.040	13
CUBS	−41.29546	174.77438	47	0.63	278	0.099	0.029	3
DAVS	−41.20579	174.95436	35	0.63	300	0.157	0.006	36
FAIS	−41.20740	174.94010	15	0.05	1000	0.089	0.003	53
FKPS	−41.28795	174.77876	30	0.41	323	0.160	0.007	50
HSSS	−41.15194	174.98148	9	0.22	526	0.060	0.004	23
INSS	−41.23352	174.92112	28	0.09	630	0.063	0.006	15
LHBS	−41.19665	174.89232	23	0.05	626	0.084	0.005	58
LHES	−41.21169	174.90334	175	1.16	222	0.148	0.009	44
LHRS	−41.20474	174.89319	0	0.05	622	0.072	0.003	54
LHUS	−41.23085	174.89364	243	1.75	212	0.126	0.008	29
LIRS	−41.23231	174.91929	16	0.25	400	0.103	0.006	40
LNBS	−41.20498	174.92660	131	0.80	330	0.097	0.004	41
LRSS	−41.22943	174.90425	200	1.72	256	0.161	0.007	26
MISS	−41.31489	174.81843	97	1.15	274	0.151	0.011	35
NBSS	−41.20227	174.95376	47	0.90	190	0.185	0.014	37
PGMS	−41.22451	174.87944	274	1.79	200	0.121	0.011	31
PHFS	−41.25265	174.90455	23	0.05	615	0.133	0.043	2
PHHS	−41.25209	174.90430	23	0.05	613	0.091	0.002	50
PIPS	−41.26749	174.78607	157	1.00	210	0.240	0.016	27
POTS	−41.27222	174.77464	24	0.24	453	0.074	0.002	74
PTOS	−41.22297	174.86030	23	0.20	450	0.072	0.005	34
PVCS	−41.22475	174.87392	296	2.00	190	0.144	0.011	29
RQGS	−41.29653	174.78115	46	0.60	246	0.100	0.021	9
SEAS	−41.32645	174.83764	53	0.30	305	0.115	0.004	47
SEVS	−41.24698	174.90216	246	1.20	209	0.165	0.007	26
SOCS	−41.20433	174.91594	151	1.35	233	0.157	0.008	37
TAIS	−41.18038	174.95477	42	0.69	510	0.127	0.004	49
TEPS	−41.29059	174.78106	103	0.99	292	0.126	0.006	38
TFSS	−41.27543	174.78305	157	1.73	271	0.177	0.010	55
TRTS	−41.29870	174.77390	29	0.28	270	0.136	0.008	44
VUWS	−41.27985	174.77840	70	0.87	286	0.198	0.007	59
WANS	−41.23121	174.93102	15	0.05	1000	0.126	0.009	28
WCFS	−41.29315	174.78479	7	0.24	349	0.005	0.005	1
WEL	−41.28405	174.76818	0	0.05	687	0.135	0.005	56
WEMS	−41.27429	174.77926	128	0.98	265	0.146	0.007	54
WNAS	−41.32641	174.80903	66	1.12	229	0.117	0.010	37
WNHS	−41.30078	174.77551	50	0.32	493	0.091	0.008	27
WNKS	−41.28482	174.74205	39	0.31	369	0.187	0.009	62
WTES	−41.28158	174.77419	7	0.09	334	0.004	0.004	1
WTYS	−41.29543	174.78126	49	0.80	230	0.018	0.007	4

Source: site metrics are based on Wotherspoon et al. (2022).
SMS: strong motion stations.
N_E = number of events used to calculate SA ratios.

Assessment of reference stations

To estimate site response from observational data, a reference site was used. For this study, the Wellington Pottery Association building SMS (POTS) was selected as the reference station and is used for computing spectral acceleration (SA) amplification factors
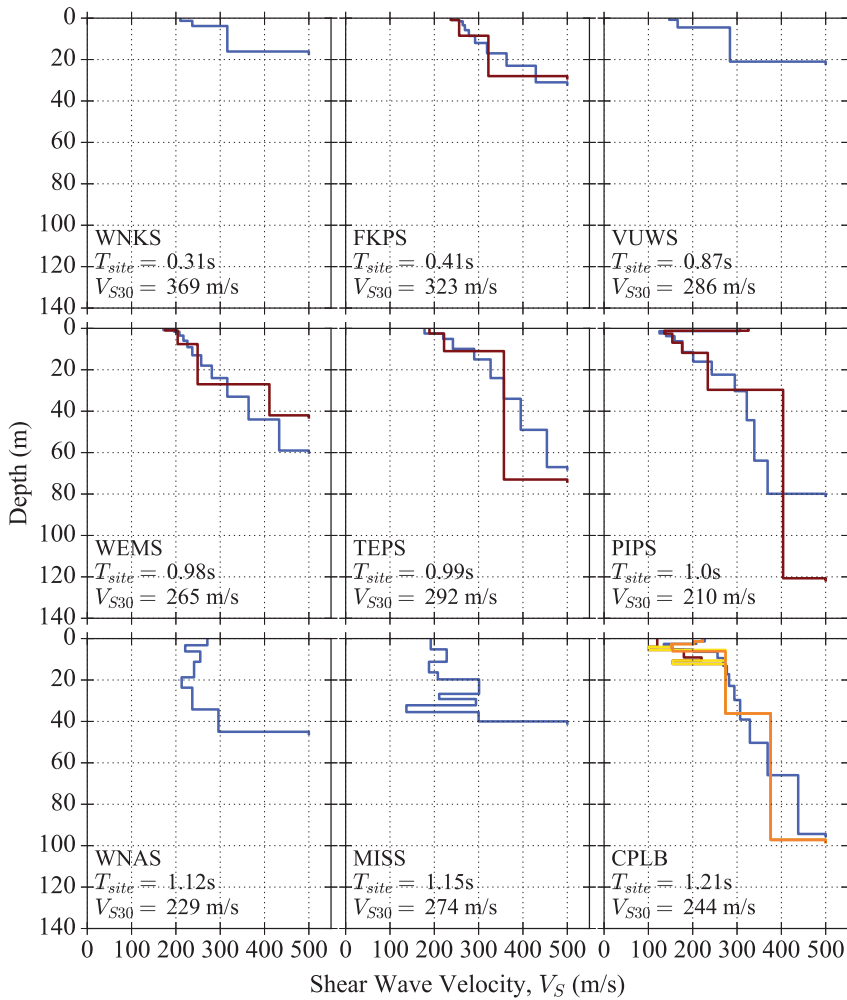
Figure 3. Shear wave velocity profiles for the nine sites at which nonlinear site-response analyses were performed. Subplots are ordered by increasing T_{site} from top-left to bottom-right.

(i.e. ratios) at all sites. As shown in Figure 2, POTS lies outside of the basin, just north of the surface trace of the Wellington Fault and at the toe of the Wellington hills. A borehole with downhole V_S measurements was performed outside of the Pottery Association building, approximately 15 m from the instrument. This was the closest feasible point for the borehole based on access constraints on the sloping ground and publicly accessible road. A site map with the locations of the instrument and borehole, which shows the local topography, is included in Figure A.1 of the electronic supplement. The measured V_S profile and site-to-site residuals ($\delta S2S$) from many empirical GMMs are also provided in Figures A.2 and A.3 of this electronic supplement, respectively.

The measured V_{S30} value at the aforementioned location 15 m from the POTS instrument is 453 m/s, and the soil profile from the borelog comprises approximately 23 m of gravelly quarry rock fill, underlain by 3 m of weathered rock, underlain by unweathered Greywacke rock. As shown in Figure A.1, the borehole was performed adjacent to the
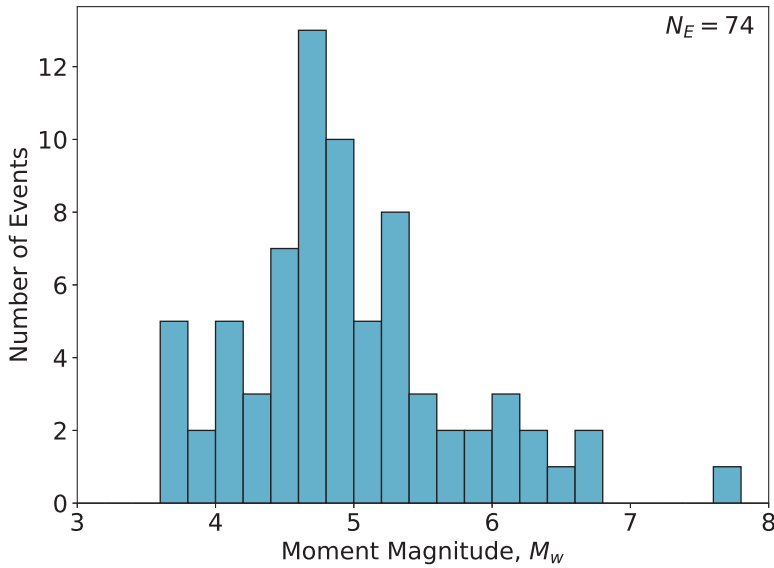
Figure 4. Histogram of moment magnitude (M_w) for all 74 events recorded at the reference station, POTS, that were used to compute observed site amplification factors.

Pottery Association building, in an in-filled gully that underlies part of the building. This gully is only approximately 10–20 m wide and has been filled with approximately 20 m of rock quarry at the northeastern edge of the building. However, the majority of Grant Rd (see Figure A.1) is cut into the hillside and has vertical cuts through weathered rock. This suggests that the soil conditions and V_S measured in the borehole at this location may not be representative of the average V_S and soil conditions under the footprint of the building, or the global site response of the area and building. It is noted that given the relatively small length scales of the gully, only high frequencies would be influenced by this fill, if at all. This article focuses most on the long-period amplification caused by sediments of the basin.

Kaiser et al. (2023) showed that estimates of full site response (i.e. site response predicted by the model plus the uncaptured site response represented by the site-to-site residual; relative to $V_{S30} = 760$m/s) using the Atkinson (2022) GMM compare well with site-response estimates calculated in this article using observations relative to the POTS station. To confirm this, we performed predictions and residual analysis using two V_{S30} values for POTS: 453 m/s (as measured in the borehole), and 760 m/s (a value hypothesized to represent the response at POTS). The site-to-site residuals from many GMMs using these two V_{S30} are plotted in Figure A.3 of the electronic supplement. This confirms that with the measured value of $V_{S30} = 453$m/s the site response at POTS is overpredicted, and that with the hypothesized values of 760 m/s, a residual closer to 0 is obtained, suggesting that perhaps the site response observed at POTS is more representative of a site with $V_{S30} = 760$m/s.

The earthquake HVSR at POTS is relatively flat (see Figure 2 of Bradley et al., 2018), suggesting that strong site effects are not present. Bradley et al. (2018) anecdotally suggested using POTS and PTOS as reference stations, based on HVSR and the similarity of
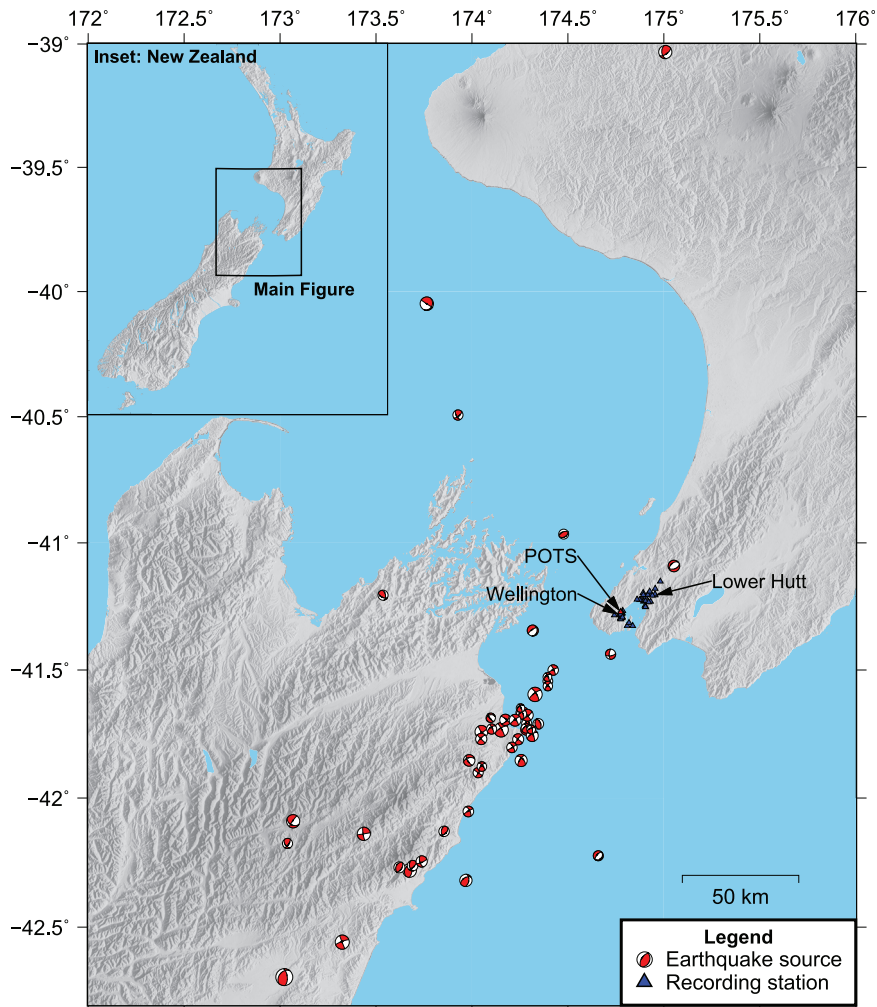
Figure 5. Map showing the location of epicenters of all events considered relative to the sites considered. The reference station, POTS, is labeled and plotted with a red triangle.
Source. The size of focal mechanism symbols are scaled to M_w of each event. As shown in the inset of New Zealand, the map encompasses the top of the South Island and the bottom of the North Island.

response spectra recorded at other rock SMS in the area. The site responses relative to POTS (i.e. the SA amplification factors) are compared in Figure 6 for several other sites outside of the basin edge and hill sites that could be considered as potential reference sites. SA for many of these sites are generally consistent, although some are likely influenced by the following effects: (1) site amplification for softer soil sites on the basin edge (WCFS, WTES, and SEAS), (2) topographic amplification at the tops or crests of hills (e.g. WANS, LHBS, and WEL; refer to topography in Figure 2), and (3) topographic deamplification at the toe of slopes (PTOS and INSS in Lower Hutt). On average, the site response at POTS is similar to other rock outcrop and stiff shallow soil sites.

POTS is located in close proximity to other sites in Wellington such that for sites in the Thorndon and Te Aro basins, distance scaling of the ground motions should not
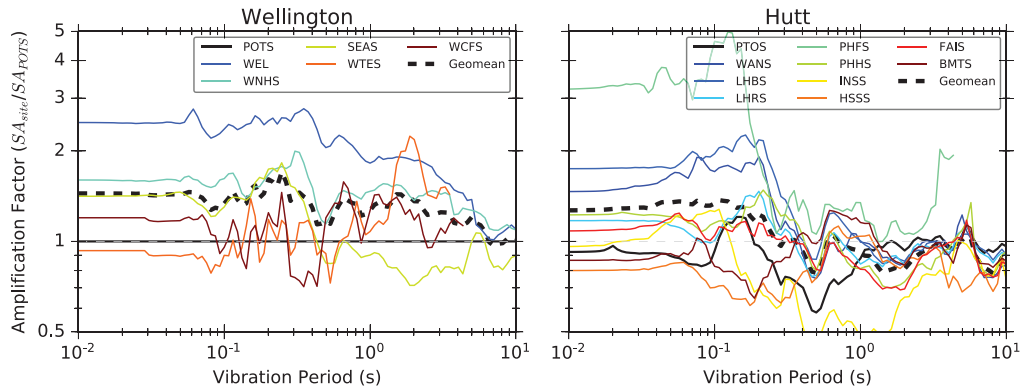
Figure 6. Geometric mean observed spectral acceleration amplification factors relative to site POTS for potential reference sites in Wellington (left) and Hutt (right). Potential reference sites are those outside the basin either on the edge of the basin (POTS, WTES, and WCFS in Wellington; PTOS and INSS in Hutt) or in the hills surrounding the basin (WEL, WNHS, SEAS in Wellington; WANS, LHBS, LHRS, PHFS, PHHS, HSSS, FAIS, and BMTS in Hutt).

significantly influence the observed amplification factors. As shown in Figure 5, the source-to-site distances are generally large compared with the distance between POTS and other sites in Wellington. For Lower Hutt sites, the distance to POTS (approximately 8–18 km) is such that there may be some influence of source-to-site distance on spectral ratios for some of the closer events located in the Cook Strait and the NE corner of the South Island. We acknowledge this limitation, but still selected POTS as the reference for all stations because (1) a direct comparison can be made between Wellington and Lower Hutt ground motion amplitudes, albeit with some influence from distance scaling, (2) all Lower Hutt sites are using the same reference and can therefore be reasonably compared between themselves, and (3) the influence of distance scaling over these distances, if any, would primarily effect short periods.

The comparison of POTS to other similar stiff shallow soil or rock stations, its proximity to sites in the Wellington area, and the assessment of HVSR data and site-to-site residuals that do not suggest that POTS experiences pronounced or unusually large site response, make it a good candidate for use as a reference station throughout this article. This station was chosen over PTOS because the larger number of events recorded at POTS and the seemingly strong deamplification observed at PTOS around $T = 0.5$ s in Figure 6.

Observed linear site amplification factors

For all 43 stations shown in Figure 2, observed site response was estimated using ratios of SA relative to the reference rock station, POTS. Geometric mean spectral ratios, or "amplification factors," of all events recorded at any station and reference station pairs were computed. As discussed in subsequent sections, the majority of events produced weak shaking with generally linear response. However, trends in amplification factors, and predictions from 1D site-response analyses and empirical models, suggest there is likely some influence from nonlinearity for the intensity of shaking corresponding to the strongest records at soft sites, albeit minor. It was chosen to keep these events in the

calculation of the linear site term in order to be able to resolve long-period amplification from larger-magnitude events. The effects of nonlinearity on observations were "removed" using results of nonlinear analyses, as discussed in the "Correcting observations for minor soil nonlinearity to compute the observed linear site response" section. The term site response used herein encompasses the combined effect from geometric amplification (i.e. basin effects) and near-surface soil amplification (e.g. impedance amplification due to soil stratigraphy, and soil response).

The top panels in Figure 7 plot geometric mean observed site amplification factors for sites within these three basins (Te Aro, Thorndon, and Lower Hutt). The results for different basins are plotted on separate columns, and lines are color-coded by the site period, T_{site}. The figure shows that shallower basin sites (i.e. Te Aro basin), with lower site period estimates, produce larger amplification at short periods (up to approximately 1 s), and smaller amplification at longer periods. As basin depth and site period increase, amplification at long periods increases dramatically, with the deepest sites near the Wellington Harbour edge in the Thorndon Basin (e.g. TFSS, CPLB, PIPS) and in Lower Hutt (e.g. PVCS, PGMS, LHUS) experiencing severe amplification (up to a factor of $4-5$) at periods between 1 and 3 s.

The middle row of Figure 7 plots predicted spectral ratios (relative to the prediction at POTS) from empirical GMMs assuming the measured V_{S30} value near POTS (453 m/s). The bottom row plots the same ratios from GMMs, but using a hypothesized higher value of $V_{S30} = 760$m/s for POTS, which gives an estimate of the site response predicted at basin sites relative to a rock site. While the GMM predicted ratios generally follow observed trends, the magnitude of amplification is significantly underestimated for the majority of sites across the full period range. The GMM ratios relative to the 760 m/s site are closer in amplitude to the observed amplification factors, albeit they still underestimate the amplification of long period peaks. The underestimation of spectral peaks over narrow frequency ranges is not unexpected, as these ergodic empirical models use site proxies such as V_{S30} and $Z_{1.0}$ to capture average site response, but naturally do not capture the site-specific effects of impedance amplification, reflection, and refraction, which result in localized peaks and troughs in an amplification function with significantly more frequency-dependent variation. The better agreement of GMM ratios when $V_{S30} = 760$m/s for the reference site, again suggests that a V_{S30} of 453 m/s for POTS may be too low to represent the global site response of the POTS building (refer to the discussion in the "Assessment of reference stations" section).

The observed site response for deeper basin sites significantly exceed the New Zealand Standard (NZS1170.5, 2004) code-based amplification factors for Site Class D (relative to a reference condition of a Site Class A/B rock site; shown as a dashed black line in Figure 7) at long periods ($1-5$ s). These sites would be classified as Site Class D under NZS1170.5 (Kaiser et al., 2020; Wotherspoon et al., 2022); therefore, the amplification function plotted in Figure 7 would be adopted in a code-based approach. Given that the observed amplification factors are based on weak motions, the question of whether these factors are appropriate for use with stronger, design-level ground motions, where soil nonlinearity is expected, is assessed in this study. It should be noted that the current NZS1170.5 amplification factors are independent of ground motion intensity.

Influence of nonlinearity on observations. While most events in the database produced weak recorded motions, the three largest magnitude and highest intensity ground motions (from
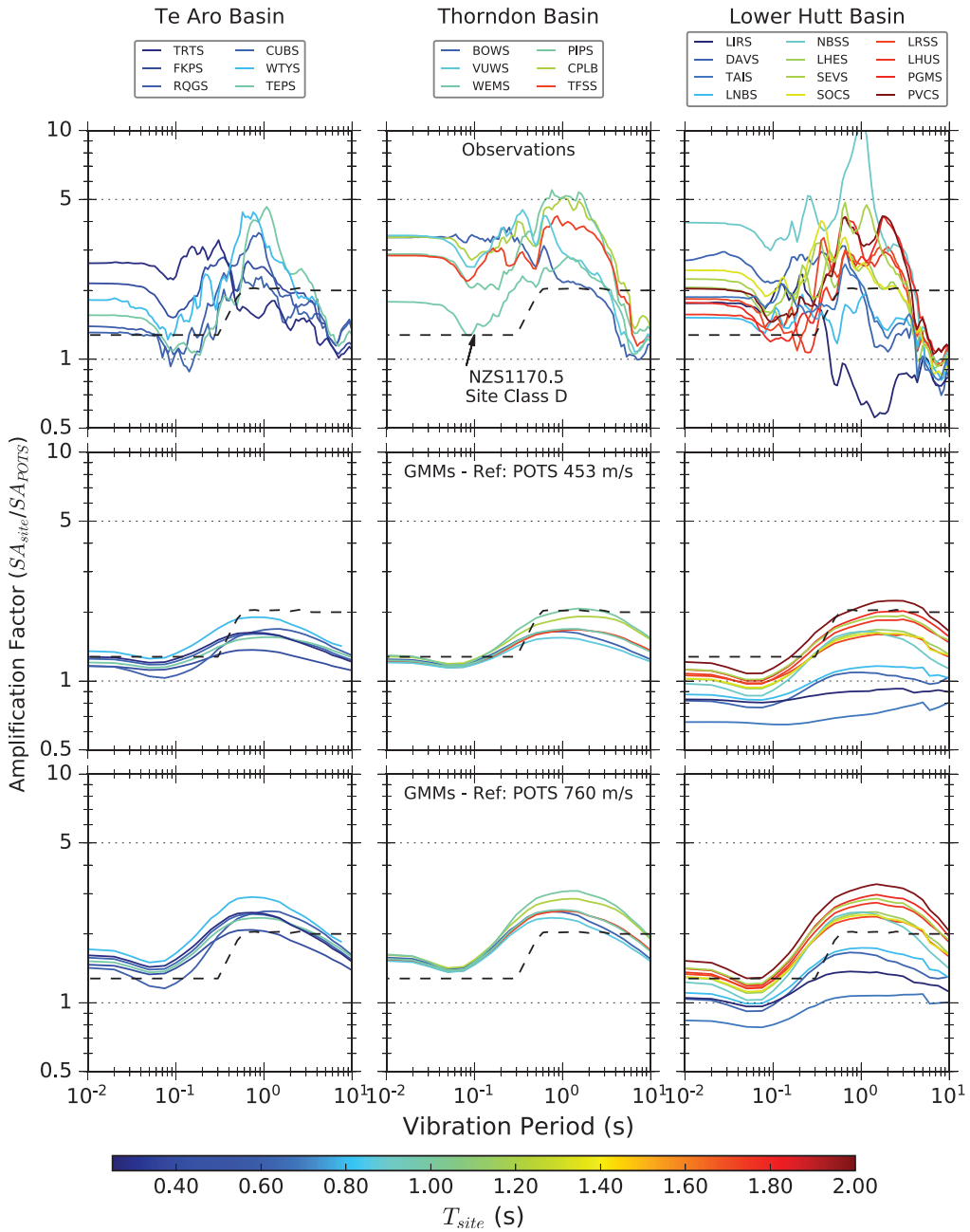
Figure 7. Geometric mean spectral acceleration amplification factors relative to the reference site POTS for: observed ground motions (top row), empirical GMM predictions using $V_{S30} = 453$m/s for POTS (middle row), and empirical GMM predictions using $V_{S30} = 760$m/s for POTS (bottom row). Sites are divided into the main three basins of interest: Te Aro Basin (left), Thorndon Basin (middle), and Lower Hutt (right). Curves are color-coded by site period. The NZS1170.5 code-based amplification factors for Site Class D is shown by the black dashed line.
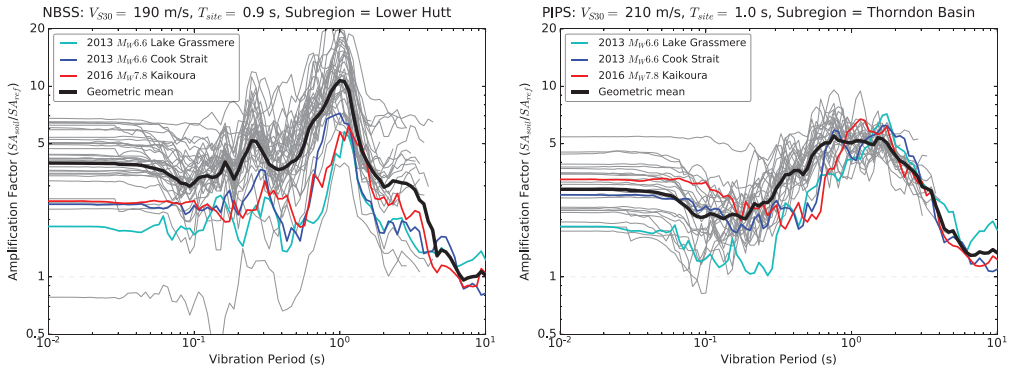
Figure 8. Observed spectral acceleration amplification factors for all events recorded at two soft soil sites: NBSS in Lower Hutt (left), and PIPS in Thorndon Basin (right). The three largest earthquakes (i.e. largest magnitude and strongest shaking intensity) are identified with different colors to illustrate potential influence of nonlinearity on observations.

the 2016 $M_w7.8$ Kaikōura, 2013 $M_w6.6$ Cook Strait, and 2013 $M_w6.6$ Lake Grassmere earthquakes) do appear to show some influence of nonlinearity at several of the softest sites. Spectral ratios for two example sites, NBSS in Lower Hutt ($V_{S30} = 190\,\text{m/s}$ and $T_{site} = 0.9\,\text{s}$) and PIPS in the Thorndon Basin ($V_{S30} = 210\,\text{m/s}$ and $T_{site} = 1.0\,\text{s}$), are plotted in Figure 8. As illustrated in these figures, most sites show remarkable event-to-event repeatability across all events. However, observations at these soft sites generally show a reduction of amplification factors, primarily at periods between $T = 0.2 - 0.8\,\text{s}$ due to soil nonlinearity for the largest three events (identified in Figure 8). As shown through simulations in the subsequent results sections, severe nonlinearity at soft sites (e.g. PIPS) would manifest as much stronger deamplification, from the weak motion or linear amplification factors, than what is observed in Figure 8.

The highest recorded peak ground accelerations (PGA) are from the Kaikōura earthquake and correspond to 0.074 g at the reference station (POTS) and about $0.2 - 0.25$ g on soft soil basin sites (see Table 1). Without observations of stronger events in these Wellington basins, there is no empirical evidence to show if such large amplification factors (especially at long periods) will still be representative when strong soil nonlinearity occurs.

Nonlinear site-response analyses

To estimate how amplification factors vary with increasing ground-motion intensity, nonlinear total stress site-response analyses were performed using strong ground motions. Two orthogonal components of ground motions for the three largest-magnitude events recorded at the reference station (POTS) were scaled to reference PGA (PGA^r) values ranging from 0.01 to 1.0 g and used as outcrop input motions to 1D nonlinear site-response models. We acknowledge the limitations due to neglecting pore pressure generation at sites that may be liquefiable (particularly sites close to the waterfront on CentrePort; see Figure 1), and from using a limited number of ground motions with a wide range of scale factors (ranging from about 0.1 to 28). More robust hazard-consistent ground-motion selection would use different ground-motion ensembles for different bins

of ground-motion intensity levels considered (e.g. Ch. 10 in Baker et al., 2021). The analyses were performed using the finite element code OpenSees and the site-response program DEEPSOIL to assess the influence of constitutive model assumptions. One of these assumptions is the use of Masing versus non-Masing unload–reload behavior in the constitutive model. In OpenSees, the pressure-dependent multi-yield (PDMY02) and pressure-independent constitutive models (PIMY) (Yang et al., 2003), which adopt Masing unload–reload behavior, were used. In DEEPSOIL the General Quadratic/Hyperbolic Model (GQ/H; Hashash et al., 2010) was coupled with a non-Masing formulation. Importantly, given the use of strong ground motions in this study, both models generate strength-based backbone curves. With PDMY02 in OpenSees, a hyperbolic backbone curve is generated based on a specified friction angle and reference pressure, and with GQ/H in DEEPSOIL, typical modulus reduction and damping (MRD) curves are matched at small strains and soil shear strength is matched at large strains. This topic is discussed in more detail in the "Maximum shear strains" section. In OpenSees, the PDMY02 model was used for sandy and gravelly layers, the PIMY model was used for soft silts and clays, and both the PIMY and PDMY02 models (in separate analyses) were used for nonplastic silt layers.

The input parameters defined in this study for the PDMY02 model in OpenSees include: soil density, friction angle, shear, and bulk moduli at a reference pressure and the reference pressure. For the phase-transformation angle and contraction/dilation parameters, the default values based on relative density from the OpenSees Wiki were used. These contraction/dilation parameters do not influence the response, because the analyses are drained (i.e. an unrealistically high value of permeability is used). For PIMY in OpenSees, only the soil density, friction angle, and shear and bulk moduli are required. For DEEPSOIL, the input parameters include layer thickness, unit weight, shear wave velocity, shear strength, and reference MRD curves. Another modeling difference between these two codes, in addition to the different Masing unload–reload behavior, is the use of a pressure-dependent constitutive model for sands and gravels in OpenSees. While this could have some influence under strong shaking for soft soils, the soil and V_S profiles used (Figure 3) are of relatively high depth resolution, which inherently accounts for the depth-dependent increase in soil stiffness and strength.

The profiles used in 1D site-response analyses were taken down to a reference condition with shear wave velocity (V_S) of 500 m/s at the halfspace. Three main reasons for selecting this reference conditions are (1) significant nonlinearity is not expected for stiffer materials (with higher V_S), (2) the 1D site-response assumption used in these analyses is not considered appropriate for greater depths in these basins where the wave field would likely be significantly 3D, and (3) the V_{S30} for the reference site, POTS, is 453 m/s. More details on the V_S profiles used for these analyses are in the "Sites considered and basins in the wellington region" section.

Combining nonlinear adjustment factors with observed amplification factors

Quantifying the effects of nonlinearity in simulations. To estimate how the linear observed basin amplification factors change with increasing ground motion amplitude, nonlinear adjustment factors are computed from results of the 1D site-response analyses. The first step is to assess how the amplification factors from simulations vary with increasing amplitude relative to a reference linear simulation with a weak motion as follows:

1. Compute the geometric mean SA amplification factor (AF) from 1D site-response analyses for input motions with $PGA^r = 0.01$ g. This is taken as the linear simulated reference $\left[AF_{lin}^{sim}(T)\right]$ for each site (e.g. the dark blue lines in Figure 10).
2. Bin the remaining amplification factors $\left[AF^{sim}(T, PGA^r)\right]$, from simulations with scaled input motions, into PGA^r bins of 0.1 g (e.g. $0.01 - 0.1$ g, $0.1 - 0.2$ g, $0.2 - 0.3$ g).
3. Calculate the geometric mean amplification factor for each PGA^r bin $\left[AF_{bin}^{sim}(T, PGA^r)\right]$.
4. Compute nonlinear adjustment factors as $F_{NL}(T, PGA^r) = AF_{bin}^{sim}(T, PGA^r)/AF_{lin}^{sim}(T)$ for each bin.
5. Use the midpoint of each PGA^r bin (e.g. 0.05, 0.15, 0.25, 0.35 g, etc.) as the representative value for the bin.
6. To calculate approximate nonlinear adjustment factors for arbitrary values of PGA^r, linearly interpolate between these midpoint values.

Correcting observations for minor soil nonlinearity to compute the observed linear site response. Once the nonlinear adjustment factors are computed from simulations, the observations were slightly corrected to back-calculate a corresponding linear amplification factor. While the observations are of relatively weak motions, and do not cause significant nonlinearity, the softest sites do experience minor soil nonlinearity effects from the strongest ground motions as explained above in the "Influence of nonlinearity on observations" section. Rather than neglecting these ground motions in computing the observed linear amplification, we chose to correct them based on simulations so that the amplification at long periods from these larger magnitude events could be included (i.e. most other events have a maximum usable period <10 s). The nonlinear adjustment factors calculated above are used to correct observations to the linear amplification factors as follows:

1. Calculate the observed SA amplification factor relative to the reference station (POTS) for every event, e, recorded at every site, s as $AF_{s,e}^{Obs}(T) = SA_{s,e}(T)/SA_{POTS,e}(T)$.
2. If PGA^r from an observation (i.e. PGA at POTS) is <0.01 g, the amplification factors are considered as linear for the event and no adjustment is applied. This applies to the majority of observations. This is a reasonable assumption based on trends in observations, simulations, and empirical GMM predictions that show little to no change in the slope of amplification factor versus PGA^r for PGA^r<0.01 g (e.g. Figure 11).
3. If PGA^r from an observation (i.e. PGA at POTS) is >0.01 g, the period-dependent nonlinear adjust factors (F_{NL}) calculated above are linearly interpolated based on the observed PGA^r and the midpoint of PGA^r bins.
4. The linear observed amplification factor (in linear scale) for each event is now back-calculated by dividing out the interpolated nonlinear adjustment factors from the "raw" amplification factor with minor effects of nonlinearity as $AF_{lin,s,e}^{Obs}(T) = AF_{s,e}^{Obs}(T)/F_{NL}(T, PGA^r)$.
5. For each site, take the geometric mean of all events to compute the observed linear site response $\left(AF_{lin,s}^{Obs}\right)$.

Adjusting observed linear site response to larger intensities based on nonlinear simulation results. After estimating the observed linear site response for each site (i.e. the geometric mean $AF_{lin,s}^{Obs}$),

the predicted amplification factors for PGA^r values up to 1 g can be calculated using the nonlinear adjustment factors calculated above as follows:

1. For each PGA^r bin, calculate the average nonlinear adjustment factor as described in the "Quantifying the effects of nonlinearity in simulations" section.
2. Multiply the linear site response term by the nonlinear adjustment factors, that is, $AF_s(T, PGA^r_{bin}) = AF^{Obs}_{lin,s}(T) \times F_{NL}(T, PGA^r_{bin})$.

Illustrative examples of this procedure and the final results for all sites at which non-linear site-response analyses were performed are in the "Modification of observed linear site response using nonlinear adjustment factors from simulations" section.

Results and discussion

Illustrative example of response spectra for increasing ground-motion intensity

To illustrate how the predicted amplification of ground motions varies with increasing input motion amplitude, response spectra for individual analyses are plotted in Figure 9. Results for different V_S profiles (see Figure 3 and the relevant discussion) and the two analysis codes are also included to demonstrate the uncertainty associated with such modeling assumptions. In this figure, and for the remainder of the article, we use two example sites to illustrate representative trends in the results. One is a stiff soil site, FKPS (left side of Figure 9), with $V_{S30} = 323$ m/s and $T_{site} = 0.41$ s, and the other, PIPS (right side of Figure 9), is a softer hydraulic fill site with $V_{S30} = 210$ m/s and $T_{site} = 1.0$ s. The figure plots response spectra of input and ground surface output motions for analyses with the 2016 M_w7.8 Kaikōura earthquake recording at POTS scaled to a PGA^r of 0.01, 0.1, and 1.0 g.

Figure 9 illustrates that under weak ground-shaking (e.g. $PGA^r = 0.01$ g), where the soil is expected to remain approximately linear, there is significantly more site amplification for the softer site (PIPS), and the amplification extends to longer periods of up to approximately 2 s. Under this level of shaking, the results from OpenSees and DEEPSOIL are practically the same, and the uncertainty from V_S profile selection is greater than that from using different softwares (i.e. constitutive model and unload/reload behavior).

As the intensity of ground-shaking increases, softer sites (such as PIPS) exhibit larger strains and more severe nonlinearity. This is visible in Figure 9, in which PIPS experiences more severe deamplification at short periods due to soil nonlinearity from the input motion with $PGA^r = 1.0$ g. At these very large strains, the uncertainty attributed to constitutive model assumptions becomes more significant than that from V_S profiles, with the DEEPSOIL analysis resulting in more severe deamplification at both sites. For this more severe ground motion, some amplification is now predicted at long periods. This occurs over a wider range for the stiffer site (FKPS) and is more pronounced for the DEEPSOIL results. These differences in results between codes may be caused by the issues discussed in the "Nonlinear site-response analyses" section, which are (1) Masing versus non-Masing unload–reload behavior, (2) pressure-dependent versus pressure-independent strength and stiffness, and (3) differences in the MRD curves.
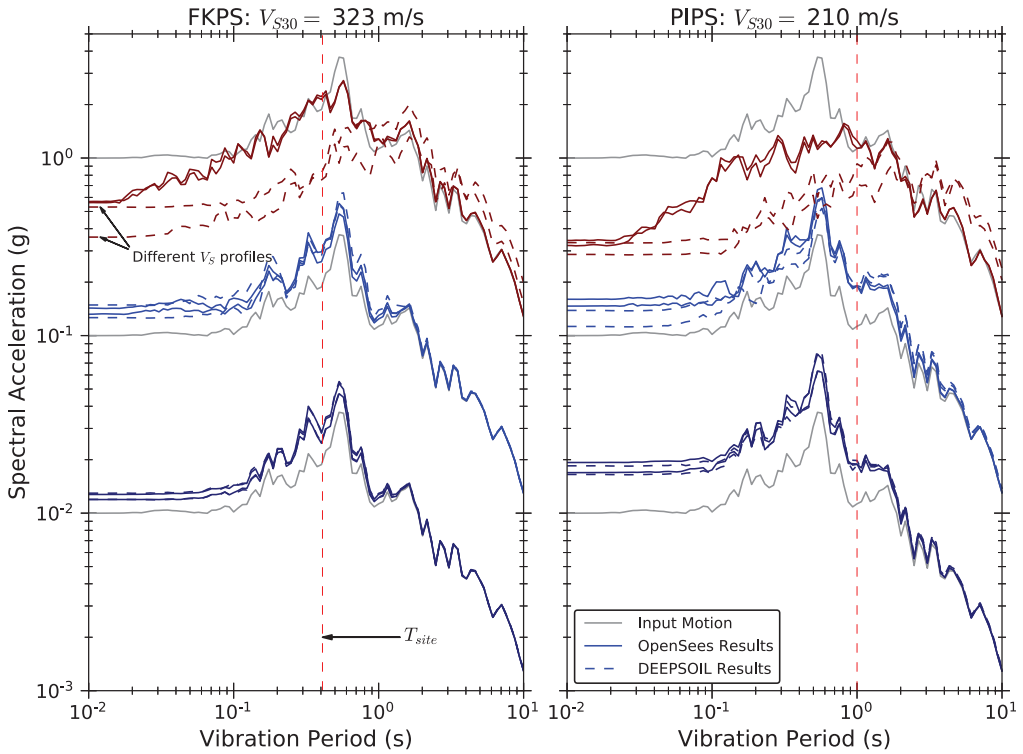
Figure 9. Example response spectra showing the influence of soil nonlinearity with increasing amplitude of the input motion (i.e. PGA^r) for a relatively stiff site (left; FKPS) and a relatively soft site (right; PIPS). For each site, input and output response spectra are plotted for analyses with the 2016 M_w7.8 Kaikōura earthquake input motions scaled to PGA^r = 0.01 (dark blue), 0.1 (blue), and 1 (dark red) g. Ground surface output response spectra are plotted for OpenSees (solid lines) and DEEPSOIL (dashed lines), with two different V_S profiles for each software.

Influence of nonlinearity on site amplification factors

The same trends discussed above for individual response spectra can also be seen in amplification factors for all analyses at a given site. To further illustrate these trends, SA amplification factors (i.e. $SA_{surface}/SA_{input}$) from 1D site-response analyses of all ground-motion intensities (PGA^r) at PIPS are plotted in Figure 10. Geometric means from observations and empirical GMM predictions are also included in the figure. In the same way that observed spectral ratios are computed for the weak-motion database, the GMM amplification factors are computed as the ratio of the GMM prediction for each site to the GMM prediction at POTS for all crustal events in the database. The majority of NGA-West2 (i.e. Abrahamson et al., 2014; Boore et al., 2014; Campbell and Bozorgnia, 2014; Chiou and Youngs, 2014) and New Zealand specific Bradley (2013) GMMs were used for these predictions.

Figure 10 illustrates that the amplification factors from 1D analyses are significantly lower than the observed median amplification factor at long periods. This is expected, as this long period energy comes from 3D effects at greater depths, not considered in 1D site-response models with limited vertical extents. However, this highlights one of the severe limitations of using nearby rock outcrop motions as input to 1D site-response analysis of
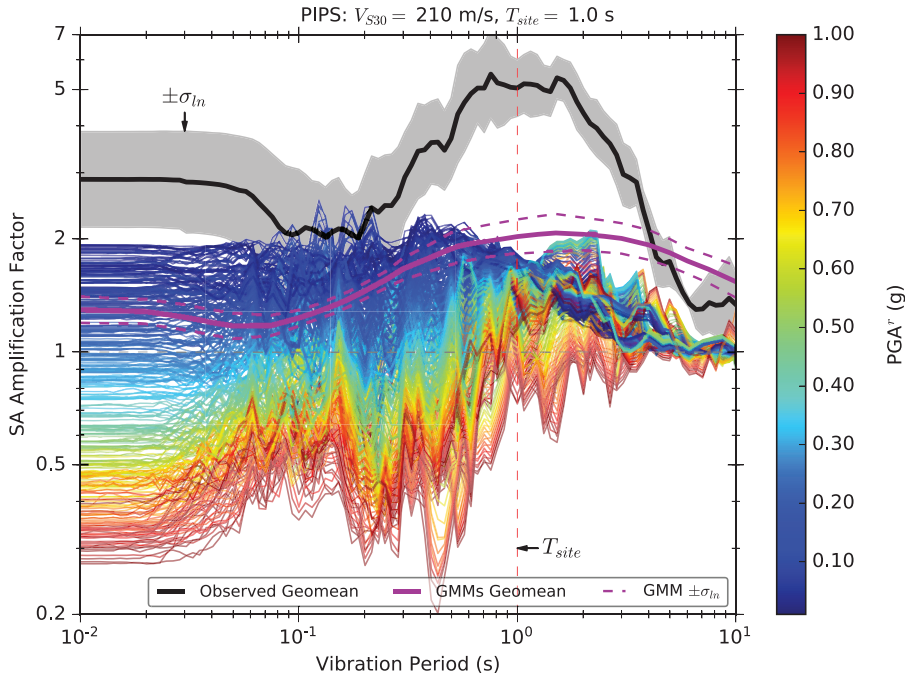
Figure 10. Comparison of spectral acceleration amplification factors for the geometric mean of observations, the geometric mean of empirical GMM predictions, and individual nonlinear analyses for all input motions with increasing intensity (ratio of soil surface motion to input motion) for an example soft site (PIPS). The nonlinear site-response results are color-coded by *PGA*r. Natural-log standard deviations for the observed amplification factors, and predictions from individual empirical GMMs are also included.

soil/basin sites (i.e. any 3D basin effects that impact nonlinearity dependence will not be considered). While this poses issues for trying to directly predict the surface motion, this article focuses more on the relative amplification between different intensity levels. Interestingly, the GMM predictions also significantly under-predict the additional long period amplification from POTS to a soft basin site. This suggests that the index parameters used to estimate site and basin amplification (e.g. V_{S30} as well as $Z_{1.0}$ and $Z_{2.5}$: the depths to $V_S = 1.0$ and 2.5 km/s, respectively) are uncertain, or are not capturing the full site amplification in these Wellington basins.

The results in Figure 10 can be viewed at individual vibration periods to effectively visualize how the amplification factors vary with increasing PGA^r. Examples of this are shown in Figures 11 and 12 for FKPS and PIPS, respectively. Amplification factors for PGA and three vibration periods are plotted versus PGA^r. Individual observations are plotted to inspect how these change with increasing observed PGA at the reference station (POTS). Results from the empirical site amplification model by Seyhan and Stewart (2014) (SS2014) are also included in these figures.

Figure 11 shows that, for FKPS, there is little effect from soil nonlinearity in observations, as the observed amplification factors are fairly constant with increasing PGA^r up to the intensities observed (PGA of 0.074 g at POTS). This is consistent with the nonlinear site-response analyses, which show little influence up to these values of PGA^r. The amplification factors at $SA(T = 1s)$ show little to no deamplification for even the largest shaking

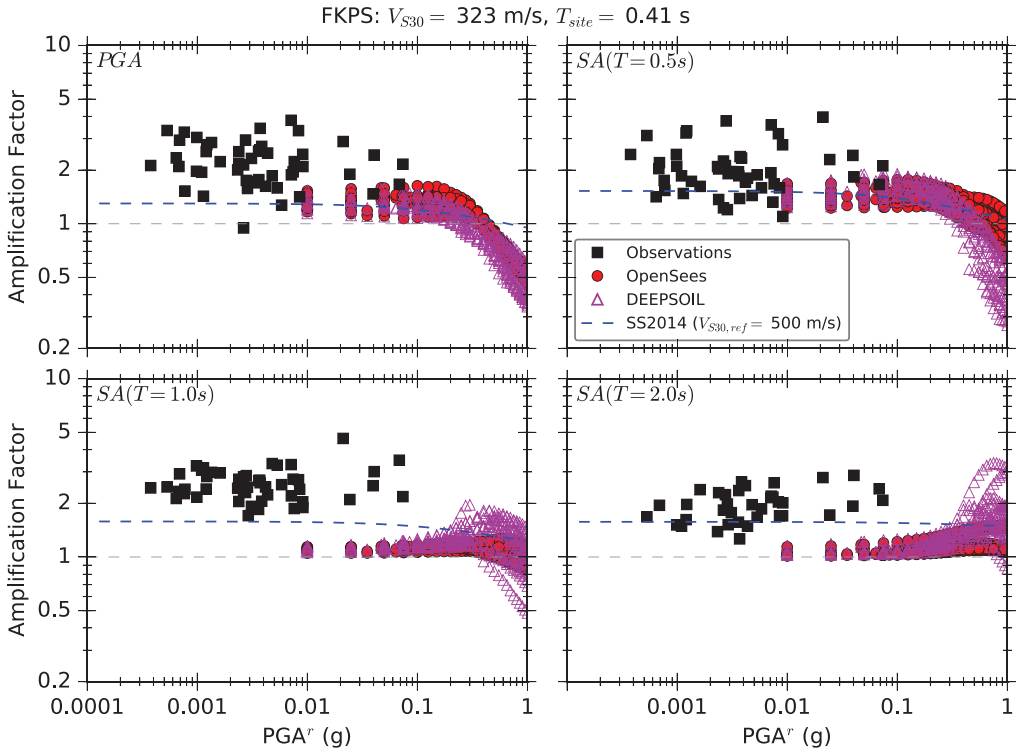**Figure 11.** Amplification factors as a function of reference motion intensity (PGA^r) for four periods (PGA, $SA(T = 0.5)$, $SA(T = 1.0)$, and $SA(T = 2.0)$). This example is for a relatively stiff site (FKPS). Results from both OpenSees and DEEPSOIL analyses are compared with observations and with predictions from the SS2014 empirical site amplification model.

intensities, and even slight amplification with DEEPSOIL for certain scenarios (i.e. V_S profile and earthquake combinations).

At PIPS (Figure 12), there is a noticeable decrease in amplification factors for observations of the three largest events at short periods (most noticeable at $SA(T = 0.5s)$ in Figure 12). Other soft sites (e.g. WNAS and MISS) also display this trend in observations at PGA and $SA(T = 0.5s)$. This trend is still consistent with results of the simulations which now, for a softer site, show some reduction of amplification factors at those levels of PGA^r. Unlike the stiffer sites, PIPS does display a reasonable decrease in amplification factors and even deamplification at $SA(T = 1s)$ for large shaking intensities.

For several sites, the 1D amplification factors at short periods provide a lower-bound estimate of the observed amplification factors calculated using POTS as a reference (e.g. PIPS, Figure 12). This is likely due to 3D basin amplification effects, and deeper impedance contrasts (e.g. soil to bedrock) that are not captured in the 1D profiles of shallow near-surface deposits (i.e. above 500 m/s), and are not present in the POTS recordings. In addition, as discussed in the "Assessment of reference stations" section, the site response at POTS may be more representative of a stiffer site than the assumed value of $V_{S30} = 453$m/s. For stiffer sites, the 1D amplification factors at short periods provide a more reasonable estimate of the median observation (e.g. FKPS, Figure 11), perhaps
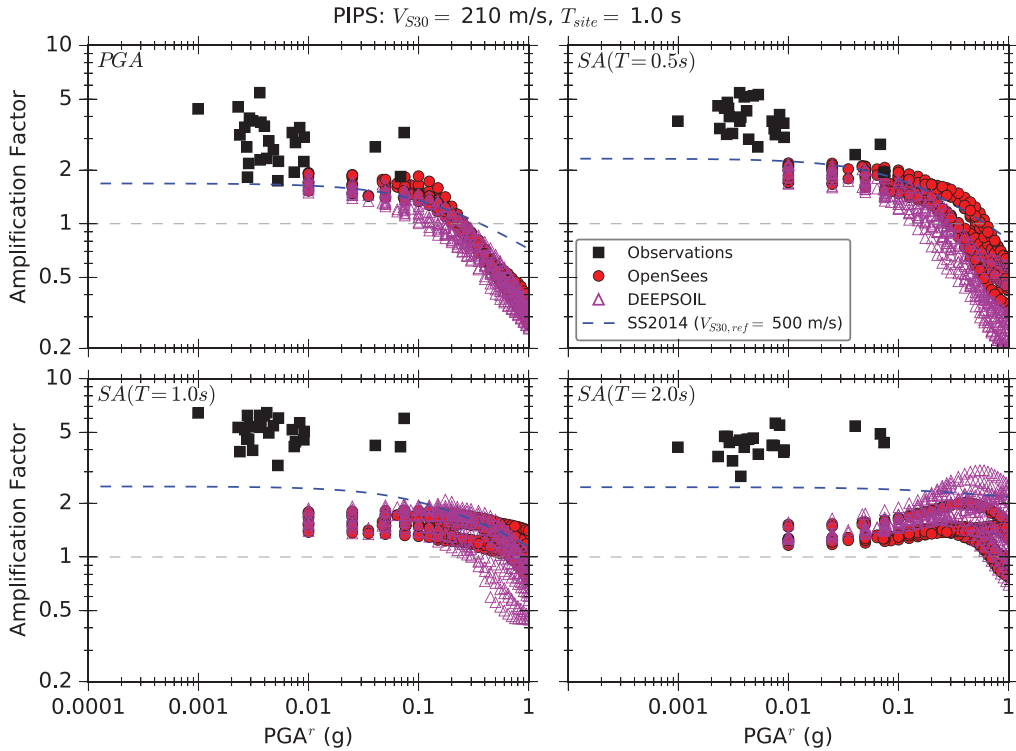
Figure 12. Amplification factors as a function of reference motion intensity (PGA^r) for four periods (PGA, $SA(T=0.5)$, $SA(T=1.0)$, and $SA(T=2.0)$). This example is for a relatively soft site (PIPS). Results from both OpenSees and DEEPSOIL analyses are compared with observations and with predictions from the SS2014 empirical site amplification model.

because the 3D amplification effects are less pronounced for these sites. As expected, for all sites, the 1D results underestimate observed long-period amplification as these analyses do not capture the deeper basin structure and 3D phenomena that contribute to this amplification.

The empirical V_{S30}-based site amplification factors (Seyhan and Stewart, 2014, included in Figures 11 and 12) match the 1D predictions well at short periods and low PGA^r values (i.e. in the elastic range). This is not the case at longer periods where the empirical model inherently accounts for deeper site response than the 1D models. At high values of PGA^r, in the highly nonlinear range, the 1D and empirical models begin to deviate significantly at short periods (PGA and $SA(T=0.5s)$ in Figure 12). The 1D analyses experience significantly more deamplification than the empirical model. For example, at PIPS, with $PGA^r = 0.5g$, the empirical model indicates an amplification factor at PGA of approximately 0.9 while the 1D nonlinear analysis predicts a value closer to 0.5. For long periods, the GMM displays a weaker dependence on PGA^r compared with the nonlinear analyses. In the highly nonlinear range, the empirical models are poorly constrained due to lack of observations, and the constitutive response becomes a challenge with greater influence in 1D site-response analyses. One of the reasons for using DEEPSOIL was to check if this severe deamplification was caused by the Masing unload/reload behavior, which has been found to overdamp the site response at large strains. As shown in these figures, the
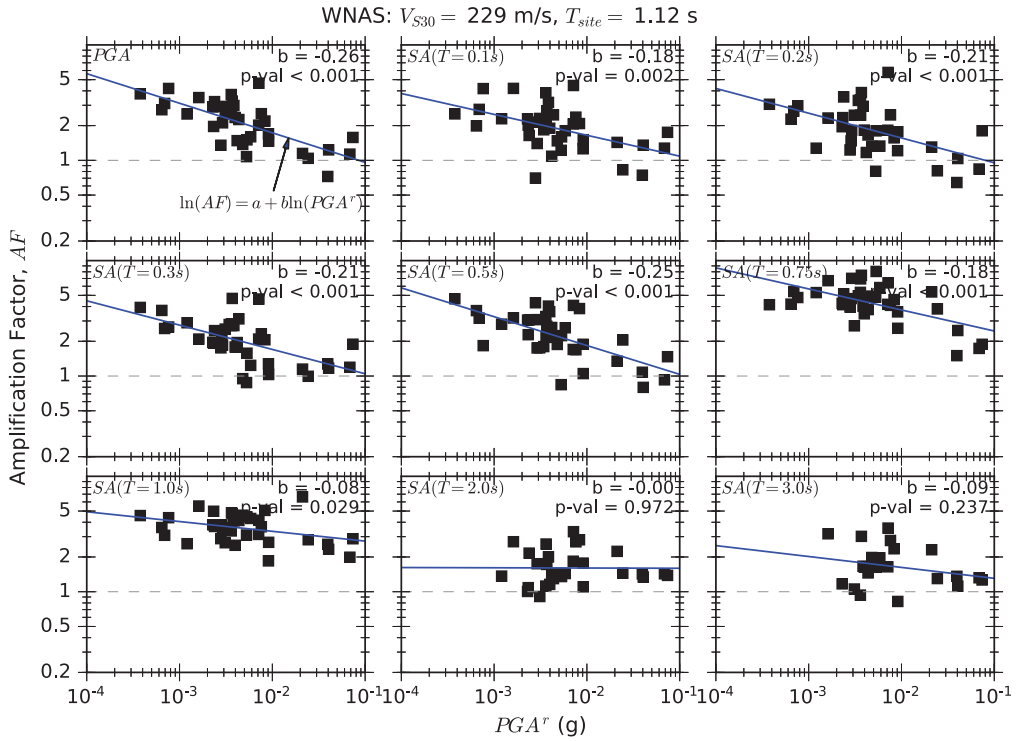
Figure 13. Example parameterization of observed amplification factors as a function of reference motion intensity (PGA^r) at nine periods for the SMS WNAS, which displays one of the strongest influences from soil nonlinearity in both observations and simulation.

Source. A linear regression is fit to the data (in natural log space) to determine the slope "*b*."

DEEPSOIL results with non-Masing assumptions still provide significant, if not more, deamplification at these high intensities. Some of the challenges of large shear strain constitutive modeling are discussed further in the "Maximum shear strains" section.

Parameterization of observed amplification factors. Further analysis of observed amplification factors was performed for all 43 sites to quantify the effects of nonlinearity as a function of ground motion intensity at various periods. Figure 13 demonstrates this relationship for nine periods at the site WNAS, where some of the strongest effects of soil nonlinearity were instrumentally observed. As seen in Figure 13, the maximum PGA recorded at POTS (i.e. PGA^r) was 0.074 g, therefore, these relationships are only appropriate for PGA^r up to approximately 0.1 g or less. A linear regression was fit to the data at every period to establish the slope of the best-fit line. This slope, *b*, which is generally negative at short periods (especially for softer sites), is proportional to the degree of soil nonlinearity expected at the site. That is, the steeper the slope, the greater the reduction in amplification factors from soil nonlinearity.

Given that the slopes (i.e. *b*) for the data in Figure 13 are indicative of the period-dependent level of nonlinearity expected at a site, this parameter should correlate well with site parameters, such as V_{S30}. Figure 14 plots *b* as a function of V_{S30} for all sites in the database that recorded more than four events (see Table 1), and these parameters are, in
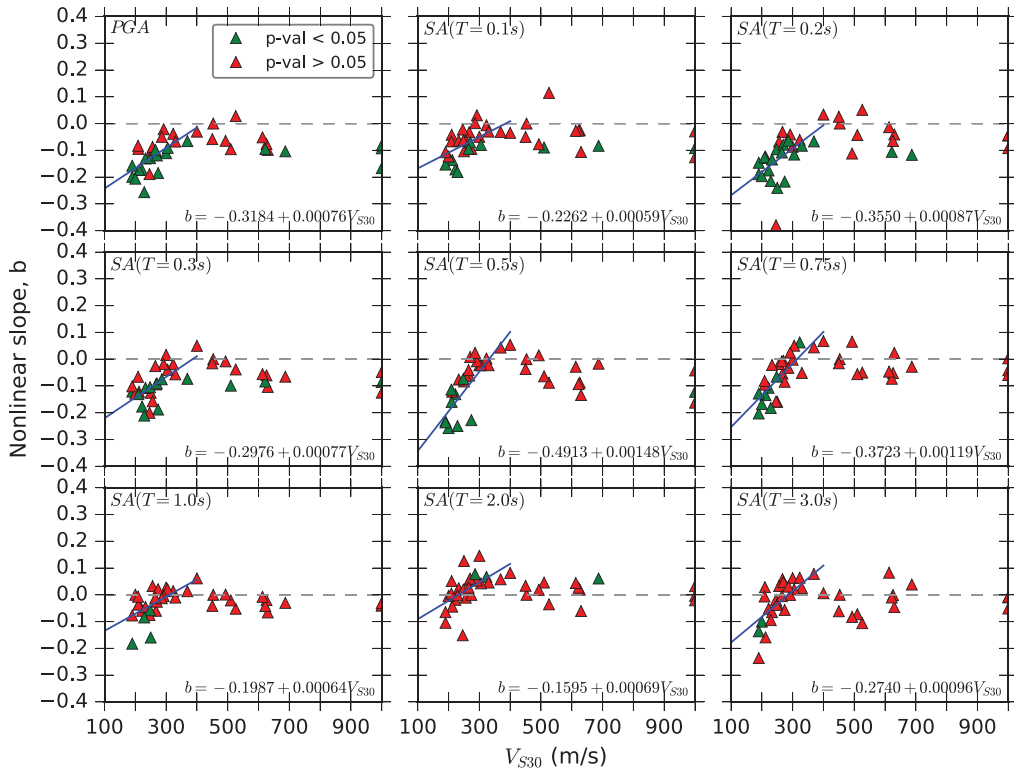
Figure 14. Nonlinear slope b (see Figure 13 for the definition of b) plotted versus V_{S30} for all sites that had more than four events. The results for nine different periods are provided (one in each sub-figure). Regressions in AF and PGA^r space that resulted in p values less than 0.05 are plotted with green markers and those with p values greater than 0.05 are plotted with red markers. The linear regression shown here in each panel was fit through all data to better illustrate trends, as a p value > 0.05 may suggest that there was negligible influence from nonlinearity at the site (i.e. there is no significant slope in AF and PGA^r space).

fact, correlated. For softer sites (i.e. lower V_{S30}), b is more negative suggesting more influence from soil nonlinearity. In the vicinity of 400 m/s, there is a breakpoint in the data, suggesting that for the intensity of ground motions observed in Wellington, there is negligible nonlinear effects for stiffer sites (at least relative to POTS). For this reason, we chose to only regress up to this value of V_{S30}. Arguably, this should be a nonlinear or bi-linear relationship for which the break point shifts to higher V_{S30} values as the intensity of ground motions considered increases. The largest negative "b" values occur at periods of $T = 0.2 - 0.75$, which is consistent with the discussion and figures in the "Influence of non-linearity on observations" section.

Maximum shear strains. One of the challenges in site-response modeling for large-strain motions, is developing constitutive models for which the behavior remains faithful to estimates of shear modulus degradation and damping (often lab-based), and soil shear strength. Even when constitutive models are capable of approximating both MRD curves simultaneously (e.g. Matasovic, 1995; Phillips and Hashash, 2008), typical curves (e.g. Darendeli, 2001) are only well constrained up to shear strains of approximately 0.3%. As
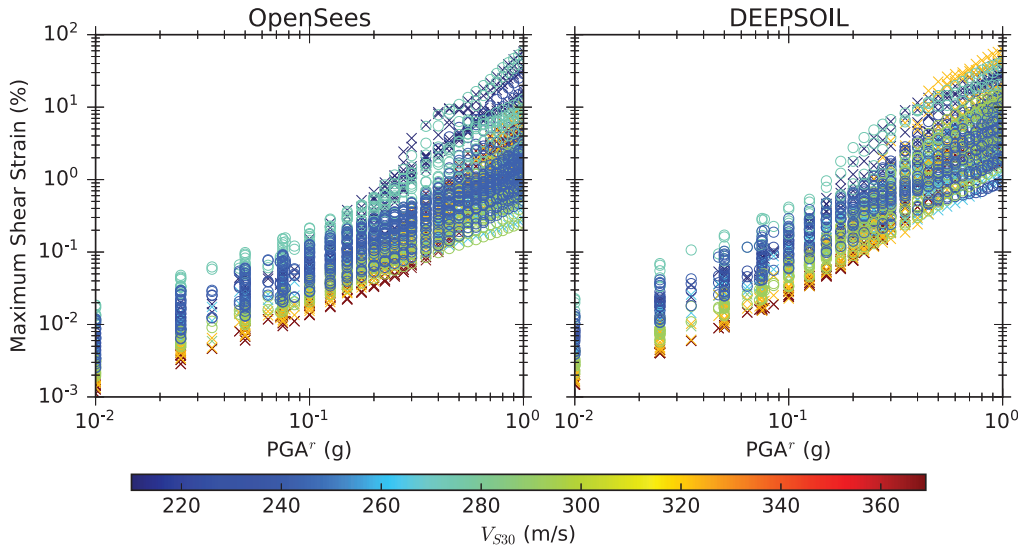
Figure 15. Maximum shear strains throughout the soil profile versus PGA^r from OpenSees (left) and DEEPSOIL (right) analyses for all sites and all input motions. Points are color-coded by V_{S30} of the site. Circle versus "x" markers are only used to help make some markers more visible.

discussed in Yee et al. (2013), when these MRD curves are extrapolated to large shear strains, they can significantly underestimate soil shear strength (i.e. the maximum shear stress that can develop in the soil). Hybrid models have been developed to honor published MRD curves at small strains and transition to strength-based hyperbolic backbone curves at large strain (e.g. Groholski et al., 2016,; implemented in DEEPSOIL).

A potential problem with using backbone curves based on typical MRD curves, which can greatly underestimate soil shear strength at large strains, is that under strong shaking the soil will fail and generate excessively large shear strains too early (i.e. at an unrealistically low shear stress; Zalachoris and Rathje, 2015). These unrealistically large shear strains may result in excessive softening and damping of the profile. The maximum value of shear strain throughout the soil profile for all sites and analyses are plotted versus PGA^r in Figure 15. These results show that even when strength-based soil backbone curves are used, very large strains (i.e. up to 10%–50%) can develop at strong input motion intensities ($PGA^r > 0.5$ g) for some sites. However, for the majority of sites and scenarios in these analyses, shear strains are below 10%.

Figure 15 shows that, in general, peak shear strain increases with decreasing V_{S30}, especially at weak levels of shaking. However, there are instances, especially for strong shaking intensities, in which a stiff site has larger shear strains than softer sites (e.g. the yellow and light green markers for stiff sites with the highest values of shear strain for DEEPSOIL and $PGA^r = 1$ g). This highlights one of the limitations of using only V_{S30} for nonlinear site-response modeling at very high shaking intensities; while the average V_S may be stiffer, other factors, such as the V_S of individual layers, and the coarseness and gradient of the V_S profile, can govern the development of shear strains in the profile.

Whether these extreme levels of maximum shear strains (1%–10%, and especially >10 %) are reasonable in site-response analyses is not well understood due to lack of field

observations and validation studies for such strong shaking and large strains. However, previous studies (e.g. Kaklamanos et al., 2015; Zalachoris and Rathje, 2015) have generally found poor performance of site-response models for peak shear strains of 0.5%–5%, with analyses under-predicting the observed amplification at short periods.

Modification of observed linear site response using nonlinear adjustment factors from simulations

The results of nonlinear site-response analyses are used nonparametrically to adjust the observed linear site response as outlined in the "Combining nonlinear adjustment factors with observed amplification factors section." Examples of the procedure and final output are shown in Figure 16 for sites FKPS (representative of stiff sites) and PIPS (representative of soft sites). The figures show results from OpenSees, DEEPSOIL, and the average of the two on three different subplots. As shown subsequently in Figure 17, the behavior at these two example sites is generally representative of the behavior of other stiff ($T_{site}<1$ s) and soft ($T_{site}>1$) sites, respectively.

For FKPS (Figure 16a), a substantial reduction in basin amplification factors, relative to the expected linear amplification, is realized up to vibration periods of about 1 s as ground-motion intensity increases. For longer periods, significant additional amplification can occur, as discussed in the previous sections. This is likely due to softening of the soil profile, resulting in elongation of the soil-profile site period and amplification of long-period energy.

For softer sites, such as PIPS (Figure 16b), severe deamplification occurs at short periods for the highest PGA^r bins, in addition to reductions in amplification factors for $T = 0.5 - 2$ s. At longer periods, nonlinearity has less effect and results in little to no additional amplification with OpenSees, and small-to-moderate amplification with DEEPSOIL, relative to the expected linear amplification. Now that the application of adjustment factors to linear site-response predictions has been demonstrated through these two examples, Figure 17 plots the value of the adjustment factor versus period for all nine sites at which nonlinear analyses were performed. From top-left to bottom-right, these subplots are ordered by increasing site period.

From Figure 17, it is evident that stiffer sites with $T_{site}<1$s and $V_{S30}>250$m/s generally behave as described above for the example of FKPS. At short periods, the adjustment factors continuously decrease with increasing ground motion intensity, and reach values as low as $0.4 - 0.6$ (i.e. a reduction in amplification factors of $60\% - 40\%$, respectively) for the highest intensity. At long periods, the adjustment factors continuously increase with increasing ground motion intensity, and reach peak values of $1.3 - 1.45$ for periods of $2 - 3$ s.

Softer sites with $T_{site}>1$s and V_{S30} generally <250m/s behave similarly to PIPS. The trend at short periods is similar to stiff sites; however, values of the adjustment factor can be as low as 0.2. The long period response is different from that of stiff sites in that the adjustment factors do not simply increase continuously with increasing intensity. For periods of about $1 - 3$ s, the adjustment factor increases to values of approximately $1.4 - 1.5$ for PGA^r of $0.35 - 0.45$ g, and then begin to decrease for higher intensities. However, for $T>3$ s, the adjustment factor does increase continuously, and reaches a maximum value of approximately 1.25 at $T = 5$ s.
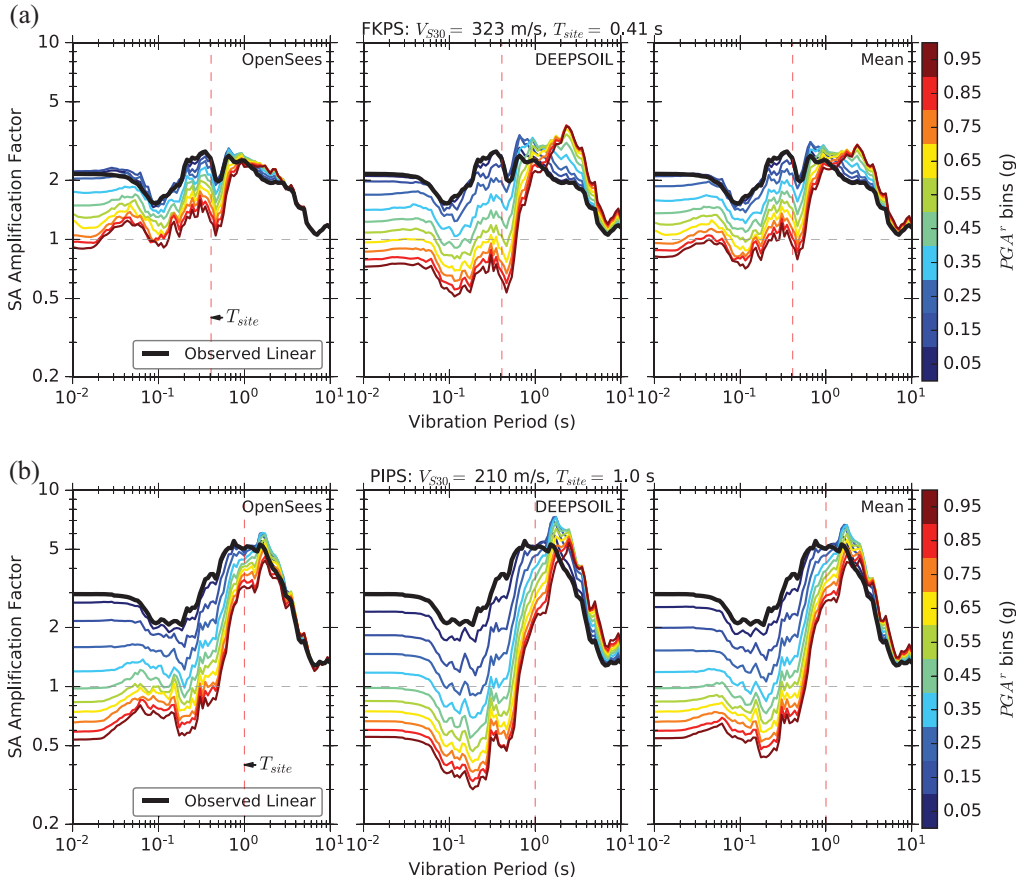
(a)

(b)

Figure 16. Spectral acceleration basin/site amplification factors computed by applying nonlinear adjustment factors from 1D site-response analyses to observed elastic basin amplification. Example results are presented for (a) a relatively stiff site (FKPS) and (b) relatively soft site (PIPS) with more severe nonlinearity. Results from OpenSees and DEEPSOIL analyses are plotted separately in addition to the average between the two codes. (a) Modified site amplification factors for a stiff site (FKPS). (b) Modified site amplification factors for a soft site (PIPS).

Now, the adjustment factors plotted in Figure 17 are applied to the observed linear amplification factors for all nine sites in Figure 18. These results represent the mean between OpenSees and DEEPSOIL analyses. For comparison, the median GMM predictions (from weak motions) with one lognormal standard deviation (σ_{ln}) bounds, and the NZS1170.5 Site Class D amplification factors for design-level motions are included. The GMM prediction ratios are relative to POTS with V_{S30} = 453m/s. Again, the subplots are organized with increasing site periods from top-left to bottom-right. For some sites (e.g. WNAS and MISS, which are underlain by a shallower and narrower sub-basin than the Te Aro and Thorndon sites, as shown in Figure 2), consideration of nonlinear effects does bring the expected amplification factors down closer to the NZS1170.5 code-based amplification factors for design-level motions. However, for sites in Thorndon and Te Aro sub-basins, amplification factors at long periods (especially for 2.0<T<5.0 s) are still significantly higher than the Site Class D factors. Importantly, for all sites, the median GMM
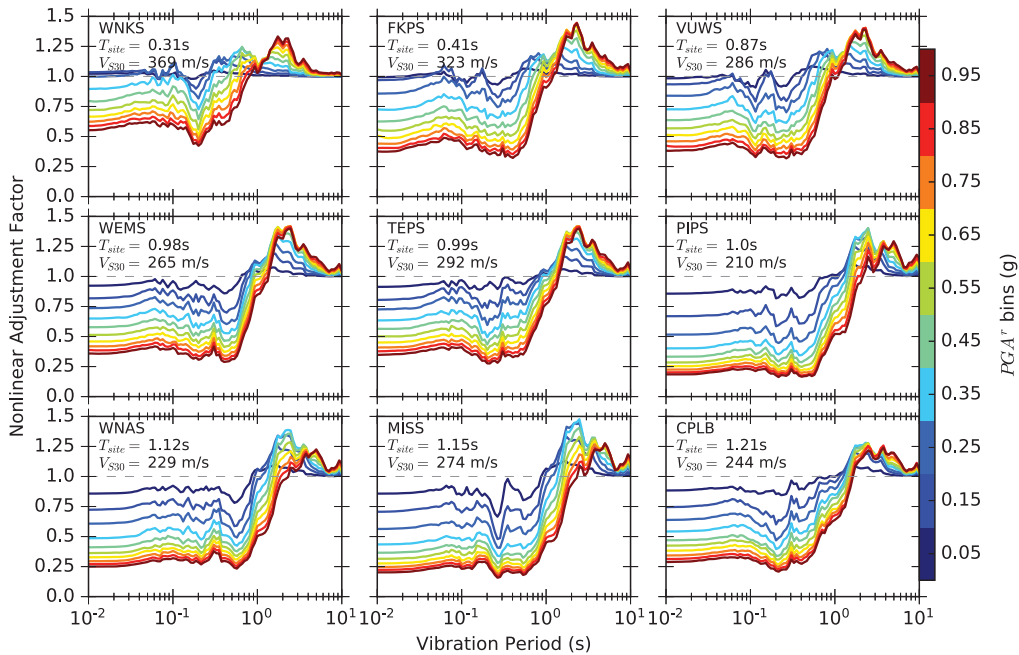
Figure 17. Nonlinear adjustment factors from 1D site-response analyses versus vibration period for all sites. The results presented here are the mean between OpenSees and DEEPSOIL analyses. Subplots are ordered by increasing T_{site} from top-left to bottom-right.

prediction underpredicts the weak-motion (i.e. essentially linear) basin amplification, especially in the period range amplified most by these basins of $0.5 - 3$ s.

Conclusion

The main objective of this study was to determine the appropriateness of using site/basin amplification factors derived from weak ground-motion observations, particularly at long periods, for strong design-level ground motions. Sites over sedimentary basins can display significant amplification at long periods under weak-ground motions, which, in many circumstances, greatly exceeds the site amplification suggested by the current New Zealand building code for Site Class D sites. Given that the soil generally remains elastic under these weak ground motions, an obvious question that arises is whether these large amplification factors should be used in combination with strong ground motions, for which soil nonlinearity is expected.

A database of weak ground motions, recorded at sites in sedimentary basins of the Wellington, New Zealand region, is used to quantify the influence of site and basin effects on the ground shaking. Given the lack of strong ground motion observations in this region, sophisticated nonlinear site-response analyses were performed with scaled input motions to understand how site amplification factors vary with increasing ground motion intensity for a range of soil conditions. A subset of nine strong motion stations with good geophysical and geotechnical site characterization data was used for these nonlinear analyses. The approach adopted here is similar to that developed in Stewart et al. (2017), albeit, we used: (1) a reference site to estimate the observed amplification as opposed to an
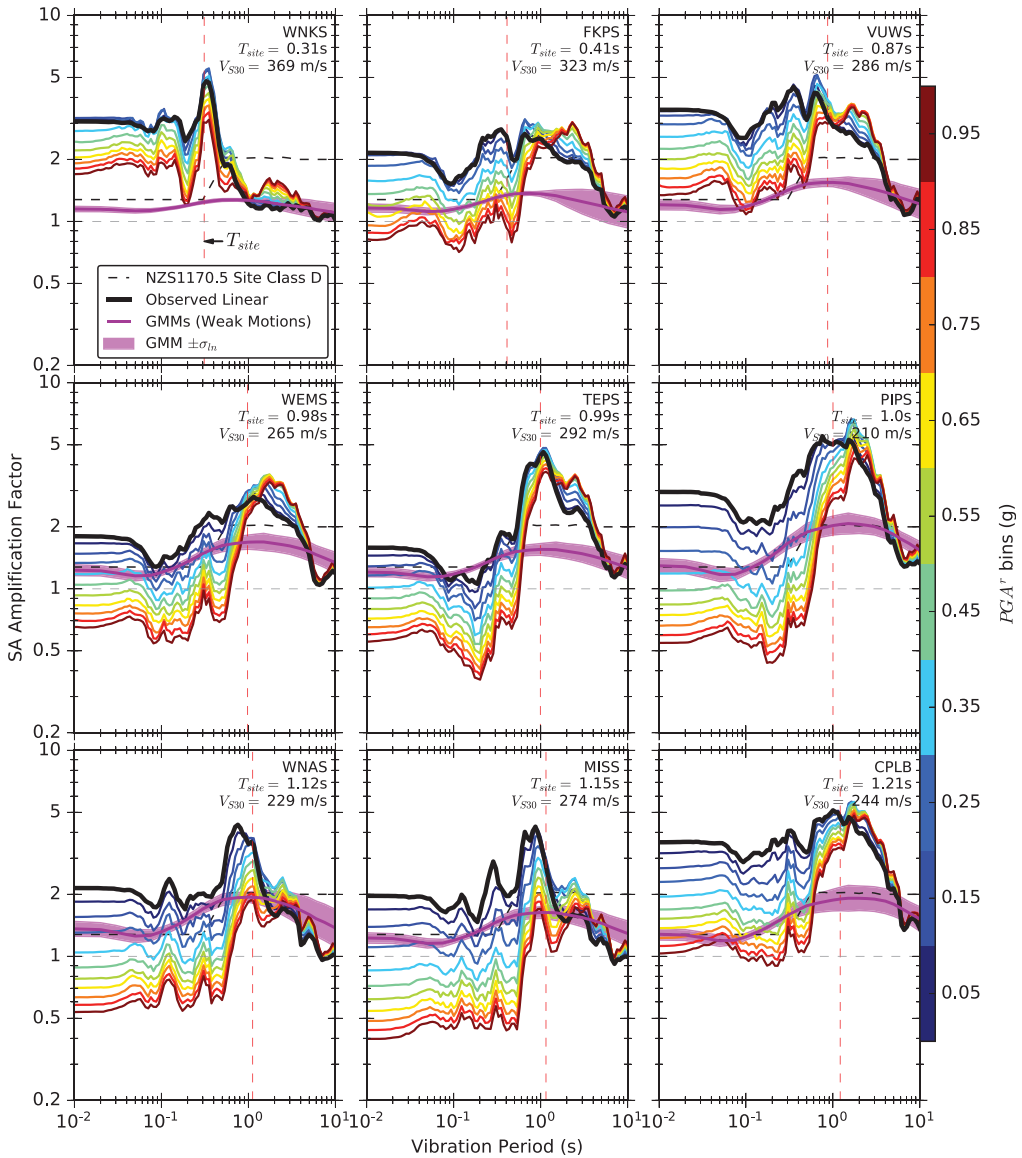
Figure 18. Spectral acceleration basin/site amplification factors computed by applying nonlinear adjustment factors from 1D site-response analyses to the estimated observed linear basin amplification for all sites. The results presented here are the mean between OpenSees and DEEPSOIL analyses. Geometric mean amplification factors predicted by empirical GMMs for the weak ground-motion database are also included.

empirical GMM and a site random effect term, and (2) a non-parameterized method as opposed to parameterization of the site amplification model from the empirical GMM.

Clear trends of increasing site/basin amplification at long periods are observed in recorded ground motions with increasing basin depth and decreasing soil stiffness. These trends in basin depth and soil stiffness correlate well with site period estimates from strong

motion stations and temporary station HVSR measurements, suggesting that site period has good predictive capabilities for site response.

Results of the nonlinear analyses suggest that, for soft sites in sedimentary basins, some reduction in SA site amplification factors at intermediate-to-long periods (i.e. 0.5–2 s) can be expected for strong ground motions due to soil nonlinearity. As an example, for the soft site PIPS (Figure 16b), the amplification factor at $SA(T = 1s)$ decreases from approximately 5 for the elastic range to approximately 3.5 for an input motion peak ground acceleration (PGA^r) of 0.5 g (i.e. a reduction of about 30%). On the contrary, for the representative stiff site FKPS (Figure 16a), which displays less site/basin amplification in the elastic range, there is little to no reduction in amplification factors at $SA(T = 1s)$, and even an increase in amplification factors for longer periods due to softening of the soil profile and site period elongation.

The results of this study show that "linear" site/basin amplification factors derived from weak ground motions should be used with discretion for strong design-level ground motions, even when considering long period amplification. We provide a method for combining such observations with site-specific nonlinear site-response analyses to develop adjustment factors to these linear-range basin terms. Given the increasing availability of seismometer or strong motion stations across many seismically active regions (including New Zealand), and the increasing use of site-specific site-response modeling in hazard predictions, the proposed approach provides a useful means to estimate combined site/basin effects for design-level seismic hazard prediction.

ORCID iDs

Christopher A de la Torre https://orcid.org/0000-0002-7946-7812
Brendon A Bradley https://orcid.org/0000-0002-4450-314X
Felipe Kuncar https://orcid.org/0000-0003-2779-2290
Robin L Lee https://orcid.org/0000-0003-1033-5923
Liam Wotherspoon https://orcid.org/0000-0002-4883-5328

Data and resources

New Zealand eScience Infrastructure's (NeSI) high-performance computing facilities and consulting support were used for all analyses and post-processing. More information is available at URL https://www.nesi.org.nz. All figures were generated in Python.

Supplemental material

Supplemental material for this article is available online.

References

Abrahamson NA, Silva WJ and Kamai R (2014) Summary of the ASK14 ground motion relation for active crustal regions. *Earthquake Spectra* 30: 1025–1055.

Adams B, Davis R, Berrill J and Taber J (2012) Two-dimensional site effects in Wellington and the Hutt Valley similarities to Kobe. *Research report, Department of Civil Engineering, University of Canterbury, Christchurch, New Zealand*, February.

Atkinson G (2022) *Backbone ground-motion models for crustal, interface, and slab earthquakes in New Zealand.* GNS Science consultancy report 2022/11, April. Lower Hutt, New Zealand: GNS Science.

Baker JW, Bradley BA and Stafford PJ (2021) *Seismic Hazard and Risk Analysis*. Cambridge: Cambridge University Press.

Bazzurro P and Cornell A (2004) Nonlinear soil-site effects in probabilistic seismic-hazard analysis. *Bulletin of the Seismological Society of America* 94: 2110–2123.

Boore DM, Stewart JP, Seyhan E and Atkinson GM (2014) NGA-West2 equations for predicting PGA, PGV, and 5% damped PSA for shallow crustal earthquakes. *Earthquake Spectra* 30: 1057–1085. doi:10.1193/070113EQS184M

Bradley B (2013) A New Zealand-specific pseudospectral acceleration ground-motion prediction equation for active shallow crustal earthquakes based on foreign models. *Bulletin of the Seismological Society of America* 103: 1801–1822.

Bradley BA, Razafindrakoto HNT and Polak V (2017) Ground motion observations from the 14 November 2016 Mw 7.8 Kaikora, New Zealand earthquake and insights from broadband simulations. *Seismological Research Letters* 88: 740–756.

Bradley BA, Wotherspoon LM, Kaiser AE, Cox BR and Jeong S (2018) Influence of site effects on observed ground motions in the Wellington region from the Mw 7.8 Kaikōura, New Zealand, Earthquake. *Bulletin of the Seismological Society of America* 108: 1722–1735.

Campbell KW and Bozorgnia Y (2014) NGA-West2 ground motion model for the average horizontal components of PGA, PGV, and 5% damped linear acceleration response spectra. *Earthquake Spectra* 30: 1087–1115.

Chiou BS and Youngs RR (2014) Update of the Chiou and Youngs NGA model for the average horizontal component of peak ground motion and response spectra. *Earthquake Spectra* 30: 1117–1153.

Cubrinovski M, Bray JD, de la Torre C, Olsen M, Bradley B, Chiaro G, Stocks E, Wotherspoon L and Krall T (2018) Liquefaction-induced damage and CPT characterization of the reclamations at CentrePort, Wellington: Liquefaction-induced damage and CPT characterization of the reclamations at CentrePort, Wellington. *Bulletin of the Seismological Society of America* 108: 1695–1708.

Darendeli MB (2001) *Development of a new family of normalized modulus reduction and material damping curves*. PhD thesis, The University of Texas at Austin, Austin, TX.

Day SM, Graves R, Bielak J, Dreger D, Larsen S, Olsen KB, Pitarka A and Ramirez-Guzman L (2019) Model for basin effects on long-period response spectra in Southern California:. *Earthquake Spectra* 24: 257–277.

de la Torre CA, Bradley BA and Lee RL (2020) Modeling nonlinear site effects in physics-based ground motion simulations of the 2010–2011 Canterbury earthquake sequence. *Earthquake Spectra* 36: 856–879.

Frankel AD, Carver DL and Williams RA (2002) Nonlinear and linear site response and basin effects in Seattle for the M 6.8 Nisqually, Washington, Earthquake. *Bulletin of the Seismological Society of America* 92: 2090–2109.

Graves R and Pitarka A (2015) Refinements to the Graves and Pitarka (2010) broadband ground-motion simulation method. *Seismological Research Letters* 86: 75–80.

Groholski DR, Asce M, Youssef Hashash MA, Asce F, Kim B, Musgrove M, Asce SM, Harmon J and Stewart JP (2016) Simplified model for small-strain nonlinearity and strength in 1D seismic site response analysis. *Journal of Geotechnical and Geoenvironmental Engineering* 142: 04016042.

Hashash YMA, Phillips C and Groholski DR (2010) Recent advances in non-linear site response analysis. In: *Fifth international conference on recent advances in geotechnical earthquake engineering and soil dynamics*, San Diego, CA, 24–29 May.

Hill M, Kaiser A, Wotherspoon L, Manea E, Lee R, de la Torre C and Bradley B (2022) *3D geologic modeling of wellington quaternary sediments and basin geometry*. GNS Science consultancy report 2022/23, September. Lower Hutt, New Zealand: GNS Science.

Hutchinson J, Dupuis M, Manea E, Bradley B, Schill C, Lee R, Motha J, Wotherspoon L and Kaiser A (2021) *2021 New Zealand ground motion database*. GNS Science consultancy report 2021/56, September. Lower Hutt, New Zealand: GNS Science.

Kaiser A, Hill M, de la Torre C, Bora S, Manea E, Wotherspoon L, Atkinson G, Lee R, Bradley B, Hulsey A, Stolte A and Gerstenberger M (2023) Overview of site/basin effects and the application of the 2022 New Zealand NSHM in Wellington, New Zealand. *Bulletin of the Seismological Society of America*. Accepted.

Kaiser A, Zhao J, Benites R, Holden C and McVerry G (2012) *It's our fault: Ground motion modelling of local site effects in the Wellington region*. GNS Science consultancy report 2012/172, August. Lower Hutt, New Zealand: GNS Science.

Kaiser AE, Hill M, McVerry G, Bourguignon S, Bruce Z, Morgenstern R, Giallini S and Wotherspoon L (2020) Wellington's sedimentary basin and it's role in amplifying earthquake ground motions: New CBD 3D model and maps. In: *New Zealand Society of Earthquake Engineering conference*, Wellington, New Zealand, 22–24 April.

Kaiser AE, Hill M, Wotherspoon L, Bourguignon S, Bruce Z, Morgenstern R and Giallini S (2019) Updated 3D *basin model* and NZS1170.5 *subsoil class and site period maps for the* Wellington CBD: Project 2017-GNS-03-NHRP. GNS Science consultancy report 2019/57, January. Lower Hutt, New Zealand: GNS Science.

Kaklamanos J, Baise LG, Thompson EM and Dorfmann L (2015) Comparison of 1D linear, equivalent-linear, and nonlinear site response models at six KiK-net validation sites. *Soil Dynamics and Earthquake Engineering* 69: 207–219.

Lee RL, Bradley BA, Stafford PJ, Graves RW and Rodriguez-Marek A (2020) Hybrid broadband ground motion simulation validation of small magnitude earthquakes in Canterbury, New Zealand. *Earthquake Spectra* 36: 673–699.

Matasovic N (1995) *Seismic response of composite horizontally-layered soil deposits*. PhD Thesis, University of California, Los Angeles, Los Angeles, CA.

Nweke CC, Eeri M, Stewart JP, Graves RW, Goulet CA and Brandenberg SJ (2022a) Validating predicted site response in sedimentary basins from 3D ground motion simulations. *Earthquake Spectra* 38: 2135–2161.

Nweke CC, Stewart JP, Wang P and Brandenberg SJ (2022b) Site response of sedimentary basins and other geomorphic provinces in southern California. *Earthquake Spectra* 38: 2341–2370.

NZS1170.5 (2004) *Structural Design Actions-Part 5: Earthquake Actions — New Zealand*. New Zealand Standards.

Parker GA and Baltay AS (2022) Empirical map-based nonergodic models of site response in the greater Los Angeles area. *Bulletin of the Seismological Society of America* 112: 1607–1629.

Phillips C and Hashash YMA (2008) A simplified constitutive model to simultaneously match modulus reduction and damping soil curves for nonlinear site response analysis. In: Zeng D,

Manzari MT and Hiltunen DR (eds) *Geotechnical Earthquake Engineering and Soil Dynamics IV*, pp. 1–10. Reston, VA: American Society of Civil Engineers.

Pilz M, Cotton F, Razafindrakoto HNT, Weatherill G and Spies T (2021) Regional broadband ground-shaking modelling over extended and thick sedimentary basins: An example from the Lower Rhine Embayment (Germany). *Bulletin of Earthquake Engineering* 19: 581–603.

Seyhan E and Stewart JP (2014) Semi-empirical nonlinear site amplification from NGAWest2 data and simulations. *Earthquake Spectra* 30: 1241–1256.

Stewart JP, Afshari K and Goulet CA (2017) Non-Ergodic site response in seismic hazard analysis. *Earthquake Spectra* 33: 1385–1414.

Vantassel J, Cox B, Wotherspoon L and Stolte A (2018) Mapping depth to bedrock, shear stiffness, and fundamental site period at CentrePort, Wellington, using surface-wave methods: Implications for local seismic site amplification. *Bulletin of the Seismological Society of America* 108: 1709–1721.

Wotherspoon L, Manea E, Bradley B, Lee R and Kaiser A (2022) National seismic hazard model: Site characterisation database summary report. GNS Science consultancy report 2022/28, September. GNS Science, Lower Hutt, New Zealand.

Yang Z, Elgamal A and Parra E (2003) Computational model for cyclic mobility and associated shear deformation. *Journal of Geotechnical and Geoenvironmental Engineering* 129: 1119–1127.

Yee E, Stewart JP and Tokimatsu K (2013) Elastic and large-strain nonlinear seismic site response from analysis of vertical array recordings. *Journal of Geotechnical and Geoenvironmental Engineering* 139: 1789–1801.

Zalachoris G and Rathje EM (2015) Evaluation of one-dimensional site response techniques using borehole arrays. *Journal of Geotechnical and Geoenvironmental Engineering* 141: 04015053.

Zhu C, Cotton F, Kawase H, Haendel A, Pilz M and Nakano K (2022) How well can we predict earthquake site response so far? Site-specific approaches. *Earthquake Spectra* 38: 1047–1075.

Zhu C, Pilz M and Cotton F (2020) Evaluation of a novel application of earthquake HVSR in site-specific amplification estimation. *Soil Dynamics and Earthquake Engineering* 139: 106301.